Optimization of Biological Production for Indian Ocean upwelling zones: Part – I: Improving Biological Parameterization via a variable Compensation Depth

Mohanan Geethalekshmi Sreeush[1,2,*].

Vinu Valsala[1],

Sreenivas Pentakota[1],

Koneru Venkata Siva Rama Prasad[2],

Raghu Murtugudde[3]

[1]Indian Institute of Tropical Meteorology, Pune, India

[2]Department of Meteorology and Physical Oceanography, Andhra University, India

[3]ESSIC, University of Maryland, USA

(*Under revision BGD*)

*Corresponding author address:
Indian Institute of Tropical Meteorology,
Dr. Homibhabha Road, Pashan, Pune 411 008, India
E-Mail: sreeushmg@tropmet.res.in

Abstract

Biological modeling approach adopted by the Ocean Carbon Cycle Model Inter-comparison Project (OCMIP-II) provided amazingly simple but surprisingly accurate rendition of the annual mean carbon cycle for the global ocean. Nonetheless, OCMIP models are known to have seasonal biases which are typically attributed to their bulk parameterization of 'compensation depth'. Utilizing the principle of minimum solar radiation for the production and its attenuation by the surface Chl-a, we have proposed a new parameterization for a spatially and temporally varying 'compensation depth' which captures the seasonality in the production zone reasonably well. This new parameterization is shown to improve the seasonality of CO_2 fluxes, surface ocean pCO_2, biological export and new production in the major upwelling zones of the Indian Ocean. The seasonally varying compensation depth enriches the nutrient concentration in the upper ocean yielding more faithful biological exports which in turn leads to an accurate seasonality in carbon cycle. The export production strengthens by ~70% over western Arabian sea during monsoon period and achieved a good balance between export and new production in the model. This underscores the importance of having a seasonal balance in model export and new production for a better representation of the seasonality of carbon cycle over upwelling regions. The study also implies that both the biological and solubility pumps play an important role in the Indian Ocean upwelling zones.

Keywords: Indian Ocean upwelling zones, Carbon cycle, Seasonal cycle - CO_2 flux and Oceanic pCO_2, Biogeochemical model parameterization, Export production - New production balance, Solubility and Biological pump.

1. Introduction

Indian Ocean is characterized by the unique seasonally reversing monsoon wind systems which act as the major physical drivers for the coastal and open ocean upwelling processes. The major upwelling systems in the Indian Ocean are (1) the western Arabian Sea (WAS; Ryther and Menzel, 1965; Smith et al., 2001; Sarma, 2004; Wiggert et al., 2005, 2006; Murtugudde et al., 2007; McCreary et al., 2009; Prasanna Kumar et al., 2010; Naqvi et al., 2010; Roxy et al., 2015) (2) the Sri Lanka Dome (SLD; Vinayachandran et al., 1998, 2004), (3) Java and Sumatra coasts (SC; Murtugudde et al., 1999; Susanto et al., 2001; Osawa et al., 2010; Xing et al., 2012) and (4) the Seychelles-Chagos thermocline ridge (SCTR; Murtugudde et al., 1999; Dilmahamod et al., 2016, Figure 1). The physical and biological processes and their variability over these key regions are inseparably tied to the strength of the monsoon winds and associated nutrient dynamics. The production and its variability over these coastal upwelling systems are a key concern for the fishing community, since they affect the day-to-day livelihood of the coastal populations (Harvell et al., 1999; Roxy et al., 2015; Praveen et al., 2016) and are important for the Indian Ocean rim countries due to their developing country status.

Arabian Sea is a highly productive coastal upwelling system characterized by phytoplankton blooms both in summer (Prasanna Kumar et al., 2001; Naqvi et al., 2003; Wiggert et al., 2005) and winter (Banse and McClain, 1986; Wiggert et al., 2000; Barber et al., 2001; Prasannakumar et al., 2001; Sarma, 2004). Arabian Sea is known for the second largest Tuna fishing region in the Indian Ocean (Lee et al., 2005). The Somali and Omani upwelling regions experience phytoplankton blooms that are prominent with Net Primary Production (NPP) exceeding 435 g C m^{-2} yr^{-1} (Liao et al., 2016). On the other hand productivity over the SLD (Vinayachandran and Yamagata, 1998), in the sea of Sri Lanka is triggered by an open ocean Ekman suction with

strong Chl-a blooms during the summer monsoon (Murtugudde et al., 1999; Vinayachandran et al., 2004). Similarly the SC upwelling is basically due to the strong alongshore winds and its variation is associated with impact of equatorial and coastal Kelvin waves (Murtugudde et al., 2000). The interannual variability associated with the Java-Sumatra coastal upwelling is strongly coupled with ENSO (El-Niño Southern Oscillation) through the Walker cell and Indonesian throughflow (Susanto et al., 2001; Valsala et al., 2011) and peaks in July through August with a potential new production of 0.1 Pg C yr^{-1} (Xing et al., 2012). The SCTR productivity has a large spatial and interannual variability. The warmer upper ocean condition associated with El Niño reduces the amplitude of subseasonal SST variability over the SCTR (Jung and Kirtman., 2016). The Chl-a concentration peaks in summer when the southeast trade winds induce mixing and initiate the upwelling of nutrient-rich water (Murtugudde et al., 1999; Wiggert et al., 2006; Vialard et al., 2009; Dilmahamod et al., 2016).

Understanding the biological production and variability in the upwelling systems is important because it gives us crucial information regarding marine ecosystem variability (Colwell, 1996; Harvell et al., 1999). The observations also provide vital insights into physical and biological interactions of the ecosystem (Naqvi et al., 2010) as well as the bio-physical feedbacks (Murtugudde et al., 2001) although limitations of sparse observations often force us to depend on models to examine the large spatio-temporal variability of the ecosystem (Valsala et al., 2013). Simple to inter-mediate complexity marine ecosystem models have been employed by several of the previous studies (Sarmiento et al., 2000; Orr et al., 2001; Matsumoto et al., 2008). However the representation of marine ecosystem with proper parameterizations in models has always been a daunting task. This is an impediment to the accurate representation of biological primary and

export productions in models (Friedrichs et al., 2006, 2007) and the issues also impact the modeling of upper trophics levels (Lehodey et al., 2010).

Biological production can be quantified with a better understanding of primary production which depends on water temperature, light and nutrient availability (Brock et al., 1993; Moisan et al., 2002) and this became the key reason for parameterizing the production in models as one or more combinations of these terms (Yamanaka et al., 2004). Any of these basic parameters can be tweaked to alter production in models. For example the availability of nutrients and light determines the phytoplankton growth (Eppely et al., 1972) or growth rate (Boyd et al., 2013). Stoichiometry and carbon-to-Chl-a ratios are other important factors to be considered in modeling (Christian et al., 2001, Wang et al., 2009) but we will not consider them in this study.

The Ocean Carbon cycle Model Intercomparison Project (OCMIP) greatly improved our understanding of global carbon cycle (Najjar and Orr, 1998). OCMIP-II further introduced a simple phosphate dependent production term in biological models for long term simulations of carbon cycle in response to anthropogenic climate change with an accurate annual mean state (Najjar and Orr, 1998; Orr et al., 2001; Doney et al., 2004). However, the OCMIP – II model simulations come with a penalty of higher seasonal biases when compared with observations (Orr et al., 2003). In this protocol the light limitation is formulated as a bulk quantity with the notion that the minimum light irradiance at which phytoplankton photosynthesis is sufficient to balance the community respiration, E_{com}, is the compensation irradiance (Sarmiento and Gruber, 2006) and the depth at which the phytoplankton photosynthesis equals whole community respiration is the community compensation depth Zc (Smetacek and Passow, 1990; Gattuso et al., 2006; Regaudix-de-Gioux and Duarte, 2010; Marra et al., 2014). Note that Zc is clearly different from the conventional euphotic zone depth (Morel, 1988). If the irradiance is less than

E_{com}, the growth will be negative, phytoplankton will decline through respiration. If the irradiance is larger than E_{com}, the planktonic photosynthesis will exceed the community respiration and production will increase (Parsons et al., 1984; Sarmiento and Gruber, 2006). Therefore the compensation depth represents the oceanic production zone in this approach. However, Zc was held constant in time and space in OCMIP-II models (Najjar and Orr, 1998; Matsumoto et al., 2008) though in reality Zc varies in space and time (Najjar and Keeling, 1997) just as the euphotic zone depth does as documented in ship measurements (Qasim, 1977, 1982). The variation in compensation depth indicates the seasonality of the production zone itself.

Most of the biophysical models prescribe a constant value for compensation depth (e.g., Zc = 75m in OCMIP –II protocol (Najjar and Orr, 1998), Zc = 100m for Minnestoa Earth System Model (Matsumoto et al., 2008). Depending on the latitude, compensation depth varies between 50m and 100m in the real world (Najjar and Keeling, 1997). In our study we have attempted a novel biological parameterization scheme for spatially and temporally varying community compensation depth in the OCMIP–II framework by representing it as a function of optimum solar radiation (Parsons et al., 1984) and Chl-a availability. In this hypothesis, the compensation irradiance is taken as 10 W m^{-2} and calculated its depth from a Chl-a attenuated solar radiation inorder to yield spatially and temporally varying Zc. Phosphate is the basic currency which limits biological production within this varying compensation depth. This spatially and temporally varying compensation depth represents the seasonality in the production zone which is lacking in OCMIP-II.

Regions of sustained upwelling like the eastern equatorial Pacific are well understood in terms of the role of upwelling in increasing the surface water pCO_2 to drive an outgassing of CO_2 into the atmosphere (Feely et al., 2001; Valsala et al., 2014). The Indian Ocean on the other hand

136 only experiences seasonal upwelling which is relatively weak in the deep tropics but stronger off
137 the coasts of Somalia and Oman and in the SLD (Valsala et al., 2013). The relative importance of
138 the solubility vs. biological pump is not well understood. Our focus here on implementing
139 seasonality in the compensation depth of OCMIP models nonetheless leads to new insights on
140 the impact of improved biological production on surface water pCO_2 and air-sea CO_2 fluxes. The
141 largely positive effects of the variable compensation depth over the Indian Ocean and the
142 sensitivity experiments where upwelling is muted strongly imply that the biological pump may
143 play as much of a role as the solubility pump in determining surface pCO_2 and CO_2 fluxes over
144 the Indian Ocean.

145 The paper is organized as follows. Model, Data and Methods are detailed in Section 2.
146 The spatially inhomogeneous Zc derived out of the new parameterization and its impact in
147 simulated seasonality of biology and carbon cycle are detailed in Section 3. Further results and
148 discussion are followed in Section 4 and a conclusion is given in Section 5.

149

150 **2. Model, Data and Methods**

151 **2.1. Model**

152 The study utilizes the Offline Ocean Tracer Transport Model (OTTM; Valsala et al., 2008)
153 coupled with OCMIP biogeochemistry model (Najjar and Orr, 1998). OTTM does not compute
154 currents and stratifications (i.e., temperature and salinity) on its own. It is capable of accepting
155 any ocean model or data-assimilated product as physical drivers. The physical drivers prescribed
156 include 4-dimensional currents (u,v), temperature, salinity, and 3-dimensional mixed layer depth,
157 surface freshwater and heat fluxes, surface wind stress and sea surface height. The resolution of

158 the model setup is similar to the parent model from which it borrows the physical drivers. With
159 the given input of Geophysical Fluid Dynamics Laboratory (GFDL) reanalysis data, the zonal
160 and meridional resolutions are 1^o with 360 grid points longitudinally and 1^o at higher latitudes but
161 having a finer resolution of 0.8^o in the tropics, with 200 latitudinal grid points, respectively. The
162 model has 50 vertical levels with 10m increment in the upper 225m and stretched vertical levels
163 below 225m. The horizontal grids are formulated in spherical co-ordinates and vertical grids are
164 in z levels. The model employs a B-grid structure in which the velocities are resolved at corners
165 of the tracer grids. The model uses a centered-in-space and centered-in-time (CSCT) numerical
166 scheme along with an Asselin-Robert filter (Asselin, 1972) to control the ripples in CSCT.

167 The tracer concentration (C) evolves with time as

168 $$\frac{\partial C}{\partial t} + U.\nabla_H C + W\frac{\partial C}{\partial z} = \frac{\partial}{\partial z}K_z\frac{\partial}{\partial z}C + \nabla_H.(K_h\nabla_H C) + \Phi \qquad (1)$$

169 where ∇_H is the horizontal gradient operator, U and W are the horizontal and vertical velocities
170 respectively. K_z is the vertical mixing coefficient, and K_h is the two-dimensional diffusion
171 tensor. Φ represents any sink or source due to the internal consumption or production of the
172 tracer as well as the emission or absorption of fluxes at the ocean surface. Here, the source and
173 sink term are provided through the biogeochemical model. Vertical mixing is resolved in the
174 model using K- profile parameterization (KPP) (Large et al., 1994).

175 In addition to KPP, the model uses a background vertical diffusion reported by Bryan and Lewis
176 (Bryan and Lewis, 1979). For horizontal mixing model incorporates Redi fluxes (Redi, 1982)
177 and GM fluxes (Gent and Mcwilliams, 1990) which represent the eddy-induced variance in the
178 mean tracer transport. A weak Laplacian diffusion is also included in the model for
179 computational stability where sharp gradient in concentration occurs.

The biogeochemical model used in the study is based on the OCMIP – II protocol as stated above. The main motivation of OCMIP–II model design is to simulate the ocean carbon cycle with a restoration approach to ocean biology using appropriate biogeochemical parameterizations. The major advantage of the OCMIP – II protocol is (i) it reproduces the first order carbon cycle and the associated elemental cycles in the ocean reasonably well and (ii) it is much easier to implement and computationally efficient than the explicit ecosystem models. The present version of the model has five prognostic variables coupled with the circulation field, viz., inorganic phosphate (PO_4^{3-}), dissolved organic phosphorous (DOP), oxygen (O_2), dissolved inorganic carbon (DIC) and alkalinity (ALK). In order to retrieve the accurate spatial and temporal distribution of CO_2 flux and pCO_2, the model uses a "nutrient restoring" approach (Najjar et al., 1992; Anderson and Sarmiento, 1995) for biological production. The basic currency for biological production in the model is phosphate because of the availability of a more extensive database and to eliminate the complexities associated with nitrogen fixation and denitrification. The biogeochemical dynamics implemented in the model and the calculations of solubility and biological pump are provided in Appendix-A

The air – sea CO_2 flux in the model is estimated by,

$$F = K_w \, \Delta \, pCO_2 \qquad (2)$$

where K_w is gas transfer velocity and $\Delta \, pCO_2$ is the difference in partial pressure of carbon dioxide between the ocean and atmosphere. The design and validation of the physical model is reported by Valsala et al., (2008, 2010) and biogeochemical design by Najjar and Orr (1998).

2.2. Data

The present setup of the model uses ocean reanalysis products based on MOM–4 (Modular Ocean Model) developed by GFDL (Chang et al., 2012). Monthly data from 1961 to 2010 were utilized in the present study. For validating the results observational datasets of CO_2 flux and pCO_2 were taken from Takahashi et al., (2009). Satellite derived Net Primary Production data were taken from Sea-viewing Wide Field of view sensor (SeaWiFS) Chl-a product, calculated using Vertically Generalized Production Model (VGPM) (Behrenfeld and Falkowski, 1997). The initial conditions for PO_4 and O_2 were taken from World Ocean Atlas (Garcia et al., 2014). Initial conditions for DIC and ALK were taken from the Global Ocean Data Analysis Project (GLODAP; Key et al., 2004) dataset. The data sources and citations are provided in the Acknowledgement.

2.3. Methods

A spin-up for 50 years from the given initial conditions is performed with the climatological physical drivers. Because the initial conditions were provided from a mean state observed climatology this duration of spin-up is sufficient to reach statistical equilibrium in the upper 1000 m (Le Quere et al., 2000). Atmospheric pCO_2 has been set to a value from the 1950s in the spin-up run for calculating the air-sea CO_2 exchange. A seasonal cycle of atmospheric pCO_2 has been prescribed.

After the spin-up, an interannual simulation for 50 years from 1961 to 2010 has been carried out with the corresponding observed atmospheric pCO_2 described in Keeling et al., (1995). The first five years of the interannual run were looped five times through the physical fields of 1961 repeatedly for a smooth merging of the spin-up restart to the interannual physical

variables. Since the study is focused only on bias corrections to the seasonal cycle with a variable Zc, a model climatology has been constructed from 1990 to 2010. This includes the anthropogenic increase of oceanic DIC in the climatological calculation and is comparable with the Takahashi et al. (2009) observations.

Additional two sensitivity experiments have been performed separately by providing annual mean currents or temperatures as drivers over selected regions of the basin for segregating the role of varying compensation depth (varZc) in improving the seasonality of carbon cycle and biological production. The model driven with annual mean currents suppress the effect of upwelling by muting the Ekman divergence over the region of interest. On the other hand, the model forced with annual mean temperatures suppresses the cooling effect of upwelling. This will highlight the effect of new parameterization in simulating seasonality of carbon cycle and biological production. A smoothing technique with linear interpolation ($u = u(1-x) + \bar{u}x$) is applied to the offline-data in order to blend the annual mean fields ($\bar{u}$) provided to the selected region with the rest of the domain (u) to reduce the sudden transition at the boundaries.

2.4. Community compensation depth (Z_c) parameterization

The OCMIP – II protocol separates the production and consumption zones by a depth termed as compensation depth (Z_c); the depth at which phytoplankton photosynthesis is large enough to balance the community respiration (i.e., both the autotrophic and heterotrophic respirations). At the community compensation depth, the Net Community Production (NCP) is zero i.e., NCP = NPP - R_h = 0, where NPP is Net Primary Production (i.e. NPP = GPP – R_a), GPP is gross

246 primary production, and R_h and Ra are the heterotrophic and autotrophic respirations,
247 respectively (Smetacek and Passow, 1990; Najjar and Orr, 1998; Gattuso et al., 2006; Regaudix-
248 de-Gioux and Duarte, 2010; Marra et al., 2014). The light intensity at compensation depth is
249 compensation irradiance (E_{com}), the irradiance at which the gross community primary production
250 balances respiratory carbon losses for the entire community (Gattuso et al., 2006; Regaudix-de-
251 Gioux and Duarte, 2010). We define a spatially and temporally varying compensation depth
252 (hereinafter varZc) as a depth where compensation irradiance (attenuated by surface Chl-a,
253 Jerlov et al., 1976) reaches a minimum value of 10 W m^{-2}. In this way the varZc has both spatio-
254 temporal variability of light as well as Chl-a. The Chl-a is given as monthly climatology as
255 constructed from the satellite data. Observations show that the primary production reduces
256 rapidly to 20% or less of the surface value below a threshold of 10 W m^{-2} (Parsons et al., 1984;
257 Ryther, 1956; Sarmiento and Gruber, 2006). Moreover higher ocean temperature (those in the
258 tropics) enhances the respiration rates resulting in high compensation irradiance (Parsons et al.,
259 1984; Ryther, 1956; Lopez-Urrutia et al., 2006; Regaudix-de-Gioux and Duarte, 2010). A study
260 by Regaudix-de-Gioux and Duarte (2010) reported the mean value of compensation irradiance of
261 Arabian Sea as 0.4 ± 0.2 mol photon m^{-2} day^{-1} which is close to 10 W m^{-2} day^{-1}.

262 Figure 2 compares the scatter of average relative photosynthesis within varZc as a
263 function of solar radiation for the Indian Ocean. This encapsulate the corresponding curve from
264 the observations for the major phytoplankton species in the ocean such as diatoms, green algae
265 and dinoflagellates (Ryther et al., 1956; Parsons et al., 1984; Sarmiento and Gruber, 2006). The
266 model permits 100% relative photosynthesis for radiation above 50 W m^{-2}. However the
267 availability of phosphate concentration in the model act as an additional limiter for production

which indirectly represents the photoinhibition at higher irradiance, for example oligotrophic gyres.

3. **Results and Discussions**

The inclusion of seasonality in Zc by way of parameterizing varZc leads to a remarkable spatio-temporal variability in compensation depth (Figure 3). The compensation depth over the Arabian Sea varies from 10 m to 25 m during December to February (DJF) and deepens up to 45 m during March to May (MAM) in par with incoming solar radiation. During the monsoon season i.e., June to September (JJAS), the compensation depth again shoals to 10 m-35 m due to the attenuation of solar radiation by the increased biological production (Chl-a). During October to November (OCT-NOV) the Zc slightly deepens as compared to JJAS.

The Bay of Bengal compensation depth deepens from 35 m to 40 m during DJF and further deepens to 50 m during MAM when the solar radiation is maximum and biological production is minimum (Prasannakumar et al., 2002). Further reduction of compensation depth can be seen through JJAS as a result of reduction in solar radiation during monsoon cloud cover. The Zc during OCT-NOV is 35 m on average. However, caution is needed since the Bay of Bengal is dominated by freshwater forcing from rivers and precipitation and temperature inversions occur routinely (Howden and Murtugudde, 2001; Vinayachandran et al., 2013). The impact of these factors on compensation depth variability is not clear and is not addressed here.

The equatorial Indian Ocean can be seen as a belt of 40 m - 45 m compensation depths throughout the season except for JJAS. During JJAS, a shallow compensation depth is seen near the coastal Arabian Sea (around 10 m to 35 m) presumably due to the coastal Chl-a blooms.

290 Deep compensation depth off the coast of Sumatra (~ 40 m to 50 m) is found during JJAS. Java-
291 Sumatra coastal upwelling is centered on September to November (Susanto et al., 2001) and
292 upwelling originates at around 100 m deep (Valsala and Maksyutov, 2010; Xing et al., 2012).

293 Southward of 10^{o}S in the oligotrophic gyre region, the compensation depth varies from 40 m to
294 more than 60 m throughout the year. A conspicuous feature observed while parameterizing the
295 solar radiation and Chl-a dependent Zc is that its maximum value never crosses 75 m especially
296 in the Indian Ocean which is the value specified in OCMIP-II models. The cutoff depth of 75 m
297 in OCMIP-II is obtained from observing the seasonal variance in the oxygen data (Najjar and
298 Keeling, 1997) as an indicator of production zone. However, our results show that
299 parameterizing a production zone based on optimum solar radiation and Chl-a (Parsons et al.,
300 1984) predicts a production zone and its variability that is largely less than 75 m. The
301 consequence of this in the seasonality of the modeled carbon cycle is illustrated as follows.

302

303 **3.1. Simulated seasonal cycle of pCO_2 and CO_2 fluxes**

304 The annual mean biases in simulated CO_2 fluxes and pCO_2 were evaluated by comparing
305 with Takahashi et al., (2009) observations (Figure 4). The model biases are significantly reduced
306 with the implementation of varZc compared to that of the constant Zc (hereinafter constZc). A
307 notable reduction in pCO_2 bias (by ~ 10µatm) is observed along the WAS (Figure 4d).

308 In order to address the role of the new biological parameterization of a variable
309 compensation depth, we extended our study by choosing four key regions where the biological
310 production and CO_2 fluxes are prominent in the Indian Ocean with additional sensitivity
311 experiments (see Introduction and references therein). The boxes we considered are, (1) Western

Arabian Sea (WAS; 40°E:65°E, 5°S:25°N) (2) Sri Lanka Dome (SLD; 81°E:90°E, 0°:10°N) (3) Seychelles-Chagos Thermocline Ridge (SCTR; 50°E:80°E, 5°S:10°S) and (4) Sumatra Coast (SC; 90°E:110°E, 0°:10°S; Figure 1). The seasonal variations of Zc over these selected key regions are shown in Figure 5. A detailed analysis of CO_2 fluxes, pCO_2, biological export and new production and the impact of varZc simulations in improving the strength of biological pump and solubility pump for these key regions are presented below.

3.2. Western Arabian Sea (WAS)

The WAS Zc has a double peak pattern over the annual cycle. Over the February-March period Zc deepens up to a maximum of 43.85 ± 2.3 m into March and then shoals to 25.75 ± 1.5 m (Figure 5) during the monsoon period (uncertainty represents the interannual standard deviations of monthly data from 1990-2010). This shoaling of compensation depth during the monsoon indicates the potential ability of the present biological parameterization to capture the wind-driven upwelling related production in the WAS. During the post monsoon period, the second deepening of compensation depth occurs during November with a maximum depth of 34.91 ± 2.2 m. The ability to represent the seasonality of biological production zone renders a unique improvement in CO_2 flux variability especially in the WAS in comparison to the OCMIP-II experiments (Orr et al, 2003; Figure 6a).

OCMIP –II simulations with a constZc of 75 m underestimate the CO_2 flux when compared to the observations of Takahashi et al. (2009). This underestimation is clearly visible during monsoon period. Our simulations with varZc result in a better seasonality of CO_2 flux when compared with Takahashi et al. (2009) observations (Figure 6a). The improvement due to varZc

scheme is able to represent the seasonality of CO_2 flux better especially during the monsoon period, when wind driven upwelling is dominant. Obviously the relative role of the biological and solubility pumps have to be deciphered in this context.

The CO_2 flux during July from observations, constZc and varZc simulations are 3.09 mol m^{-2} yr^{-1}, 1.82 ± 0.4 mol m^{-2} yr^{-1} and 3.10 ± 0.5 mol m^{-2} yr^{-1}, respectively. Southwesterly wind-driven upwelling over the WAS especially off the Somali coast (Smith and Codispoti, 1980; Schott, 1983; Smith, 1984) and Oman (Bruce, 1974; Smith and Bottero, 1977; Swallow, 1984; Bauer et al., 1991), pulls nutrient-rich subsurface waters closer to the surface while the available turbulent energy due to the strong winds leads to mixed layer entrainment of the nutrients resulting in a strong surface phytoplankton bloom (Krey and Babenerd, 1976; Banse, 1987; Bauer, 1991; Brock et al, 1991). This regional bloom extends over 700 km offshore from the Omani coast due to upward Ekman pumping driven by strong, positive wind-stress curl to the northwest of the low level jet axis and the offshore advection (Bauer et al., 1991; Brock et al., 1991; Brock and McClain, 1992a, b; Murtugudde and Busalacchi, 1999, Valsala, 2009) resulting in strong outgassing of CO_2 flux and an enhanced pCO_2 in the WAS (Valsala and Maksyutov, 2013; Sarma et al., 2002). The seasonal mean CO_2 flux during the southwest monsoon period (JJAS) for constZc and varZc simulations are 1.44 ± 0.2 mol m^{-2} yr^{-1} and 2.31 ± 0.4 mol m^{-2} yr^{-1}, respectively. The biological parameterization of varying compensation depth considerably improves the average CO_2 flux during the monsoon period by 0.86 ± 0.1 mol m^{-2} yr^{-1}. The annual mean CO_2 flux from observations, constZc and varZc simulations are 0.94 mol m^{-2} yr^{-1}, 0.80 ± 0.17 mol m^{-2} yr^{-1} and 1.07 ± 0.2 mol m^{-2} yr^{-1}, respectively. The annual mean CO_2 flux improved by 0.27 ± 0.05 mol m^{-2} yr^{-1}.

Seasonality in pCO_2 also shows a remarkable improvement during the southwest monsoon period (Figure 6b). The pCO_2 with constZc is considerably lower at a value of 385.22 ± 3.5 µatm during June compared to observational values of 392.83 µatm. However, varZc simulation perform better in terms of pCO_2 variability. The peak value of pCO_2 reaches up to 405.42 ± 5.8 µatm. The seasonal mean pCO_2 during the Southwest monsoon period from observations, constZc and varZc simulations are 397.58 µatm, 389.18 ± 3.6 µatm and 399.95 ± 5.0 µatm, respectively. The improvement in pCO_2 by varZc simulation is 10.76 ± 1.3 µatm when compared with the constZc simulation. This inherently says that constZc simulation fail to capture the pCO_2 driven by upwelling during the Southwest monsoon while varZc simulation is demonstrably better in representing this seasonal increase. The annual mean pCO_2 from observations, constZc and varZc simulations are 394.69 µatm, 389.62 ± 3.9 µatm and 391.19 ± 4.7 µatm, respectively. However it is worth mentioning that there are parts of the year where the constZc performs better compared to varZc. For instance during MAM as well as in November, the constZc simulation yielded a better comparison with the observed pCO_2 whereas varZc simulation yield a reduced magnitude of pCO_2. This may well indicate the biological vs. solubility pump controls on pCO_2 during the intermonsoons. The role of mesoscale variability in the ocean dynamics may also play a role (Valsala and Murtugudde, 2015). Nevertheless during the most important season (JJAS) when the pCO_2, CO_2 fluxes and biological production are found to be dominant in the Arabian Sea, the varZc produces a better simulation.

The improvements shown by the implementation of new biological parameterization in the simulation of CO_2 flux and pCO_2 can be elicited by further analysis of the model biological production. Figure 7 shows the comparison of model export production and new production with observational export production from satellite-derived NPP for constZc and varZc simulations.

The model export production in the constZc simulation is much weaker when compared to varZc simulation. The varZc simulation have improved the model export production. Theoretically, the new and export productions in the model should be in balance with each other (Eppley and Peterson, 1979). The constZc export production is much weaker than new production and it is not in balance. In contrast the varZc simulation yields a nice balance among them.

Comparing with the observational export production which peaks in August at a value of 154.78 g C m^{-2} yr^{-1}, the varZc simulated export and new productions peak at a value of 160.44 ± 20.4 g C m^{-2} yr^{-1} and 167.18 ± 24.0 g C m^{-2} yr^{-1}, respectively, but in July. A similar peak can be observed in constZc simulated new production as well at a value of 178.19 ± 28.0 g C m^{-2} yr^{-1}. This apparent shift of one month during JJAS in the model export production as well as in the new production is noted as a caveat in the present set up which will need further investigation. Arabian Sea production is not just limited by nutrients but also the dust inputs (Wiggert et al., 2006). The dust induced primary production in the WAS, especially over the Oman coast is noted during August (Liao et al., 2016). The mesoscale variability in the circulation and its impact on production and carbon cycle are also a limiting factor in this model as noted above.

The seasonal mean export production during the Southwest monsoon period from satellite-derived estimate is 123.57 g C m^{-2} yr^{-1}, whereas for constZc and varZc simulations it is 84.81 ± 16.0 g C m^{-2} yr^{-1} and 147.19 ± 23.8 g C m^{-2} yr^{-1}, respectively. The new biological parameterization strengthens the model export production by 62.38 ± 7.8 g C m^{-2} yr^{-1} for the Southwest monsoon period, which is over a 70% increase. This indicates a considerable impact of the biological pump in the model simulated CO_2 flux and pCO_2 over the WAS. For constZc simulation, the computed new production is slightly higher (150.84 ± 27.9 g C m^{-2} yr^{-1}) than that of varZc (133.03 ± 19.5 g C m^{-2} yr^{-1}). The annual mean export production from observations,

constZc and varZc simulations are 94.31 g C m^{-2} yr^{-1}, 77.41 ± 15.1 g C m^{-2} yr^{-1} and 122.54 ± 25.2 g C m^{-2} yr^{-1}, respectively.

To understand how the varying compensation depth parameterization strengthens the export production in the model, we analyzed the phosphate profiles. It appears that the varZc parameterization allows more phosphate concentration (Figure 8a, b) in the production zone and thereby increases the corresponding biological production (Figure 8c, d). The net export production in the model during JJAS is consistent with the satellite data (Figure 8d, see also Figure 7b). However, in the constZc case the exports are rather 'flat' throughout the season with imperfect representation of seasonal biological export. The Table 1-4 summarizes all the values discussed here.

The impact of varZc in the biological and solubility pumps is computed as per Louanchi et al., (1996, see Appendix A). The varZc parameterization has strengthens the biological as well as the solubility pump in the model and thereby modifying the phosphate profiles and achieves a seasonal balance in export versus new production (Figure 9a). During the monsoon period the varZc simulation increase the strength of the solubility and biological pumps by 10.43 ± 1.3 g C m^{-2} yr^{-1} and 106.52 ± 9 g C m^{-2} yr^{-1}, respectively (see Table 5 and 6). Similarly, the annual mean strength of solubility pump and biological pump is increased by 3.29 ± 0.6 g C m^{-2} yr^{-1} and 81.18 ± 9.92 g C m^{-2} yr^{-1}, respectively. This supports the fact that the varZc parameterization basically modifies the biological and solubility pumps in the model simulation and thereby improved the seasonal cycle of CO_2 flux and pCO_2.

3.3 Sri Lanka Dome (SLD)

The seasonal variation in the compensation depth for the SLD has a similar pattern as that of the WAS. The compensation depth deepens to its maximum during March up to 45.23 ± 0.3 m and reaches its minimum during the following monsoon period at 30.79 ± 1.5 m (Figure 5). The similarities of varZc between WAS and SLD indicate that they both are under similar cycles of solar influx and biological production. The SLD chl-a dominates only up to July (Vinayachandran et al., 2004) which explains why production with varZc increases earlier compared to the WAS which occurs during August-October.

The seasonality in CO_2 flux and pCO_2 were compared with Takahashi et al., (2009) observations (Figure 10). The varZc results in a slight improvement in CO_2 flux when compared with constZc (Figure 10a). However, both constZc and varZc simulations underestimate the magnitude of CO_2 flux when compared with observations. The seasonal mean CO_2 flux during the monsoon period is 1.79 mol m^{-2} yr^{-1} from observations, which means SLD region is a source of CO_2. But the mean values of constZc and varZc simulations yield flux values of -0.008 ± 0.2 mol m^{-2} yr^{-1} and 0.24 ± 0.2 mol m^{-2} yr^{-1}, respectively. The constZc simulation misrepresent the SLD region as a sink of CO_2 during monsoon period which is opposite to that of observations. The varZc simulations correct this misrepresentation to a source albeit at a smaller magnitude by 0.24 ± 0.09 mol m^{-2} yr^{-1} for the monsoon period. Compared to observations, the varZc case underestimates the magnitude of JJAS mean by 1.55 mol m^{-2} yr^{-1}.

The annual mean CO_2 fluxes for constZc and varZc simulations are -0.02 ± 0.1 mol m^{-2} yr^{-1} and 0.10 ± 0.2 mol m^{-2} yr^{-1}, respectively. The varZc parameterization leads to an improvement of 0.13 ± 0.1 mol m^{-2} yr^{-1} in the annual mean CO_2 flux when compared with constZc simulation. The observational annual mean of CO_2 flux is 0.80 mol m^{-2} yr^{-1} which is highly underestimated by both simulations. This indicates a regulation of biological production of the region by varZc

which makes this region a source of CO_2 during monsoon. The role of the solubility pump may also be underestimated due to the biases in the physical drivers and the lack of mesoscale eddy activities in these simulations (Prasanna Kumar et al., 2002; Valsala and Murtugudde, 2015).

The seasonality of pCO_2 (Figure 10b) especially in the monsoon period has significantly improved. The mean pCO_2 during the monsoon season from observation over the SLD region is 382.44 µatm. The seasonal mean pCO_2 during monsoon period for constZc and varZc simulations are 371.67 ± 6.04 µatm and 379.24 ± 8.9 µatm, respectively. The annual mean pCO_2 from observations, constZc and varZc simulations are 380.21 µatm, 370.76 ± 6.1 µatm and 374.94 ± 9.6 µatm, respectively. varZc simulations improve the JJAS mean pCO_2 by 7.56 ± 2.8 µatm and the annual mean pCO_2 by 4.18 ± 3.5 µatm, which is reflected in CO_2 flux as well. This is likely due to the impact of new biological parameterization in capturing the episodic upwelling in the SLD region which is further investigated by looking at its biological production.

The SLD biological production is highly exaggerated by the model for both constZc and varZc simulations (Figure 11a, b). The seasonal mean biological export for the monsoon period is 51.54 g C m^{-2} yr^{-1} as per satellite-derived estimates. However, the constZc and varZc simulations overestimate it at 167.71 ± 59.04 g C m^{-2} yr^{-1} and 151.51 ± 46.4 g C m^{-2} yr^{-1}, respectively. This exaggerated export is visible in climatological annual means where for constZc and varZc simulations they are 144.43 ± 49.8 g C m^{-2} yr^{-1} and 156.08 ± 43.8 g C m^{-2} yr^{-1}, respectively.

For constZc simulation, new production is overestimated from March to October when compared to observations and the second peak is observed in November (Figure 11a). But the overestimate in new production with varZc is observed only during JJAS period by a value of

469 26.23 g C m^{-2} yr^{-1}. For the SLD region the varZc parameterization overestimates the export
470 production but minimizes the excess new production, especially in the monsoon period by 64.15
471 ± 36.4 g C m^{-2} yr^{-1}. This indicates that the varZc parameterization is somewhat successful in
472 capturing the upwelling episode during monsoon over SLD. All values are summarized in Table
473 1-4.

474 The solubility and biological pumps are modified by the varZc parameterization significantly
475 when compared with the constZc simulation (Figure 9b). Over the monsoon period the strength
476 of the solubility and biological pumps are improved by 2.81 ± 1.1 g C m^{-2} yr^{-1} and 66.68 ± 9.7 g
477 C m^{-2} yr^{-1}, respectively. Similarly the annual mean strength of solubility and biological pump are
478 increased by 0.99 ± 1.2 g C m^{-2} yr^{-1} and 52.5 ± 5.1 g C m^{-2} yr^{-1} respectively. All values are
479 provided in Table 5 and 6.

480

481 **3.4 Sumatra Coast (SC)**

482 The seasonal variation in the compensation depth over the SC region lies between 40 m and
483 46 m (Figure 5). The seasonal maximum occurs during January to March, especially in March
484 with a depth of 45.5 m. During the monsoon period the compensation depth shoals slightly with
485 a minimum of 41.1 m in July. The variation in Zc is relatively small as compared to the other
486 regions which is consistent with its relatively low production throughout the year.

487 The seasonality of CO_2 flux and pCO_2 captured by constZc and varZc simulations are shown
488 in Figure 12a, b. The varZc simulations overestimate both CO_2 flux and pCO_2, especially during
489 the monsoon. It is found that the constZc simulation is better compared to varZc simulation. The
490 varZc simulation overestimate the seasonal mean CO_2 flux and pCO_2 by 1.19 mol m^{-2} yr^{-1} and

491 29.61 µatm, respectively, compared to observations (Table 1). However, constZc produces a
492 better estimate compared with observations for CO_2 flux and pCO_2. The constZc simulation
493 deliver a better annual mean than varZc (Table 1, 2). The annual mean bias in constZc and varZc
494 simulations for CO_2 flux is -0.0033 mol m^{-2} yr^{-1} and 0.31 mol m^{-2} yr^{-1}, respectively. Similarly,
495 pCO_2 bias is 1.95 µatm and 9.07 µatm for constZc and varZc simulations.

496 Biological production simulated by the model along SC explains the overestimation of CO_2
497 flux and pCO_2 (Figure 13). Both constZc and varZc simulations greatly overestimate export
498 production in the model. But a small enhancement in the new production during JJAS in constZc
499 case is an indicator of upwelling episodes. The seasonal mean new production during the
500 monsoon from constZc and varZc are 63.64 ± 30.9 g C m^{-2} yr^{-1} and 78.11 ± 29.1 g C m^{-2} yr^{-1},
501 respectively (Table 4). The seasonal mean export production during the monsoon from
502 observations is 58.87 g C m^{-2} yr^{-1} (Table 3). The constZc simulation represent a better new
503 production, which is seen as a relatively small exaggeration of CO_2 flux and pCO_2. The
504 biological response off SC is found to be better with constZc which is in contradiction to a
505 general improvement found with varZc in the other regions examined here. Such discrepancies
506 over the SC could be due to the effect of Indonesian Throughflow (Bates et al., 2006) which is
507 not completely resolved in the model due to coarse spatial resolution (also see Valsala et al.,
508 2010).

509 The overestimation of export production by varZc simulation is also evident by the increase
510 in strength of the biological and solubility pumps, respectively (Figure 9c). The annual mean and
511 JJAS mean DIC increases in the production zone due to the biological pump is 67.21 ± 1.3 g C
512 m^{-2} yr^{-1} and 83.62 ± 0.5 g C m^{-2} yr^{-1}, respectively. Similarly the increase in DIC due to the effect

513 of solubility pump during the JJAS period and annual mean are 10.95 ± 5.2 g C m^{-2} yr^{-1} and 3.87
514 ± 2.2 g C m^{-2} yr^{-1} respectively (see table 5 and 6).

515

516 **3.5 Seychelles-Chagos Thermocline Ridge (SCTR)**

517 The SCTR is a unique open-ocean upwelling region with a prominent variability in air-sea
518 interactions (Xie et al., 2002). Wind-driven mixing and upwelling of subsurface nutrient rich
519 water play a major role in biological production of this region (Dilmahamod et al., 2016). The
520 seasonal cycle in compensation depth is shown in Figure 5. The maximum compensation depth
521 occurs in November at about 44.94 m and the minimum at 33.2 m in July. The shoaling of
522 compensation depth during the monsoon period shows that the biological parameterization
523 captures the upwelling response over this region.

524 The seasonality of CO_2 flux and pCO_2 are shown in Figure 14. The Takahashi observations
525 of CO_2 flux shows a peak in June with outgassing of CO_2 during the upwelling episodes.
526 However, both constZc and varZc simulations underestimate this variability. The seasonality of
527 CO_2 flux in varZc shows a significant improvement when compared to constZc simulation, but
528 underestimated when compared to observations. The seasonal mean CO_2 flux during the
529 monsoon from observations, constZc and varZc simulations are 0.82 mol m^{-2} yr^{-1}, -0.32 ± 0.3
530 mol m^{-2} yr^{-1} and -0.05 ± 0.4 mol m^{-2} yr^{-1}, respectively. This represents a reduction in the seasonal
531 mean sink of CO_2 flux in the SCTR region during the monsoon by 0.27 ± 0.1 mol m^{-2} yr^{-1}
532 bringing it closer to a source region (see Table 1 for details).

533 The improved CO_2 flux is also supported by the seasonal cycle in pCO_2 . Based on
534 observations, seasonal mean of pCO_2 with constZc during JJAS is underestimated by 11.47

µatm, varZc simulation underestimate it by 6.45 µatm. So it is evident that varZc simulation capture the upwelling episodes better, marked by a larger pCO_2 during JJAS period. However, the magnitude of pCO_2 is still underestimated compared to observations (Table 2).

Figure 15 shows the biological production of constZc and varZc simulations for SCTR. It is clear that both simulations overestimate the export production and underestimate the new production. The JJAS mean export production from observations, constZc and varZc are 51.08 g C m^{-2} yr^{-1}, 57.39 ± 14.2 g C m^{-2} yr^{-1} and 99.23 ± 29.8 g C m^{-2} yr^{-1}, respectively. The varZc simulations exaggerate the model export production by 48.14 g C m^{-2} yr^{-1}. The varZc simulation improve the JJAS mean new production by 1.14 ± 2.2 g C m^{-2} yr^{-1} (Table 4). The DIC variations due to the biological pump over the monsoon period and the annual mean also support the exaggerated export production. During the monsoon period, the varZc simulation strengthen the biological and solubilitiy pump by 72.64 ± 6.2 g C m^{-2} yr^{-1} and -4.56 ± 1.6 g C m^{-2} yr^{-1}, respectively when compared to the constZc simulation (Figure 9d). This is also reflected in the annual mean DIC variations due to the biological and solubility pump effects (see table 5 and 6). This slight improvement in the model new production, especially during the monsoon period signals that the spatially and temporally varying compensation depth better captures the upwelling over SCTR. Considering the annual mean values of model export and new production, constZc simulation are reasonably faithful to observations.

The underestimation of CO_2 and pCO_2 as well as the exaggeration of model export production and a slight overestimate in model new production may be due to two reasons. (1) SCTR is a strongly coupled region with remote forcing of the mixed layer – thermocline interactions (Zhou et al., 2008) which can affect the seasonality in biological production that the model may not be resolving reasonably, (2) the bias associated with physical drivers, especially

558 wind stress may underestimate the CO_2 flux as well biological production. A similar
559 overestimation of biological production was also reported in a coupled biophysical model
560 (Dilmahamod et al., 2016).

561 Table 1 – 4 shows the entire summary of seasonal and annual mean CO_2 flux, pCO_2 and
562 biological production reported in Section 3.

563

564 **4. Sensitivity Simulations**

565 From the analysis of four major upwelling regions over Indian Ocean, it is evident that the
566 biological parameterization of spatio-temporally varying compensation depth better captures
567 upwelling episodes and thus it enhances the model export production. This is most clearly
568 visible over the WAS. In order to quantify how much the varZc parameterization contributes to
569 the seasonality of carbon cycle, two additional sensitivity simulations were carried out; (1) with
570 annual mean offline currents and (2) annual mean offline temperatures with the goal of
571 suppressing the dynamical and thermodynamical effects of seasonal upwelling over the WAS
572 (see Section 2 for details). The focus on this region is motivated by its prominence as the most
573 productive zone of the Indian Ocean. Moreover, the improvement in the biological processes in
574 the model by the varZc parameterization is best captured in this region. The results are discussed
575 below.

576

577 **4.1 Impact of varZc parameterization on seasonality of carbon cycle with annual**
578 **mean currents.**

To quantify the impact of varZc parameterization, the model is forced with annual mean currents only over the WAS with unaltered currents in the rest of the ocean. The hypothesis is that the muting of the seasonal variability of Ekman divergence removes the upwelling and the biological pump contribution to production and carbon cycle. The comparison of constZc and varZc then allows us to decipher the impact of varZc on capturing the impacts of upwelling on biological production and the carbon cycle. The smooth blending of currents at the boundary of the WAS domain is achieved by a linear smoothing function as given in Section 2.

The model biological responses (inferred by comparing with the control run) in terms of the CO_2 flux shows a flat pattern over the monsoon period for constZc simulation (Figure 16a). While the varZc simulation forced with the annual mean currents shows an enhanced CO_2 flux indicating the outgassing of CO_2 flux in the WAS due to wind-driven upwelling (Figure 16b). This qualitatively shows that the spatially and temporally varying compensation depth itself has improved the seasonality in the biological processes (export and new production) and captured the upwelling episodes during the monsoon. The varZc parameterization is responsible for an improvement of 0.48 ± 0.04 mol m^{-2} yr^{-1} and 0.13 ± 0.02 mol m^{-2} yr^{-1} in the JJAS seasonal and annual mean CO_2 fluxes, respectively. This improves the overall model CO_2 flux in the control run especially in July (Figure 16b).

Similar improvements are also noticed in pCO_2 (Figure 17). In the constZc simulation with annual mean currents, the pCO_2 dips down during JJAS monsoon period which indicates the inadequacy of constZc in capturing the upwelling enriched pCO_2 difference (Figure 17a, b). The varZc simulation slightly modifies the pCO_2 in the 'right' direction during JJAS despite the annual mean currents.

601 The export and new productions in the model explain the modification of CO_2 flux and
602 pCO_2 by varZc parameterization. The biological export production is highly underestimated in
603 the constZc simulation forced with annual mean currents while the varZc simulation captures the
604 seasonal upswing in production (Figure 18). The improved JJAS mean and annual mean export
605 production by 43.51 ± 8.6 g C m^{-2} yr^{-1} and 30.28 ± 13.7 g C m^{-2} yr^{-1}, respectively is a clear
606 indication of the positive impacts of a varZc. Similarly the improvement in JJAS mean and
607 annual mean new production (Figure 19) from varZc simulated with annual mean currents are
608 17.39 ± 0.8 g C m^{-2} yr^{-1} and 14.81 ± 0.1 g C m^{-2} yr^{-1}, respectively. In short the varZc biological
609 parameterization improves the export and new productions in the model. This helps the model to
610 capture the upwelling episodes over the study regions. Table 7 summarizes all the results of
611 biological sensitivity runs.

612

613 **4.2 Impact of varZc parameterization on seasonality of carbon cyle with annual**
614 **mean temperatures.**

615 Using the annual mean temperature over the WAS, we are suppressing the cooling effect of
616 temperature due to upwelling and quantifying how much the model seasonality is improved due
617 to varZc parameterization. (see Section 2 for details). The varZc simulations forced with annual
618 mean SST has larger JJAS mean and annual mean CO_2 fluxes by 0.88 ± 0.1 mol m^{-2} yr^{-1} and 0.28
619 ± 0.07 mol m^{-2} yr^{-1}, respectively (Figure 20 and Table 8). For a given annual mean SST the
620 solubility pump largely controls the CO_2 emission during JJAS if a varZc is prescribed, likely by
621 the enrichment of DIC (inferred from Figure 8b). Similarly the improvement in pCO_2 (Figure 21)
622 with varZc simulation is also remarkable. The JJAS mean and annual mean improvements from

623 the implementation of varZc are 11.05 ± 1.9 µatm and 1.91 ± 1.4 µatm, respectively. The
624 detailed quantification of CO_2 and pCO_2 responses for this experimental setup is given in Table
625 8. The above analysis adds supporting evidence that the varZc simulation strengthen the
626 seasonality of the model compared to the constZc case. This is presumably accomplished by the
627 more accurate compensation depth and production zone implied with a variable Zc.

628

629 **5. Summary and Conclusions**

630 A spatially and temporally varying compensation depth parameterization as a function of
631 solar radiation and Chl-a is implemented in the biological pump model of OCMIP-II for a
632 detailed analysis of biological fluxes in the upwelling zones of the Indian Ocean. The varZc
633 parameterization improves the seasonality of model CO_2 flux and pCO_2 variability, especially
634 during the monsoon period. A significant improvement is observed in WAS where the monsoon
635 wind-driven upwelling dominates biological production. The magnitude of CO_2 flux matches
636 with observations, especially in July when monsoon winds are at their peak. Monsoon triggers
637 upwelling in SLD as well which acts as a source of CO_2 to the atmosphere. The seasonal and
638 annual mean are underestimated with constZc and the SLD is reduced to a sink of CO_2 flux. The
639 varZc simulation modify the seasonal and annual means of CO_2 flux of SLD and depict it as a
640 source of CO_2 especially during the monsoon, but the magnitude is still underestimated
641 compared to Takahashi et al. (2009) observations. The SCTR variability is underestimated by
642 both constZc and varZc simulations, portraying it as a CO_2 sink region whereas observations
643 over the monsoon period indicate that the thermocline ridge driven by the open ocean wind-

644 stress curl is in fact an oceanic source of CO_2. However, the varZc simulation reduces the
645 magnitude of the sink in this region bringing it relatively closer to observations.

646 VarZc biological parameterization strengthens the export and new productions in the model,
647 which allows it to represent a better seasonal cycle of CO_2 flux and pCO_2 over the study regions.
648 The WAS export production is remarkably improved by 62.37 ± 7.8 g C m^{-2} yr^{-1} compared to
649 constZc. This supports our conclusion that the varZc parameterization increases the strength of
650 biological export in the model. Over the SLD, the JJAS seasonal mean export and new
651 productions are underestimated in varZc compared to constZc simulations, but the annual mean
652 export production is improved. Export production at SC and SCTR are highly exaggerated and
653 there is hardly any improvement in new production with a variable Zc especially over the
654 monsoon period. The inability of varZc parameterization to improve the seasonality of SC and
655 SCTR may be due to the interannnual variability of biological production associated with the
656 Indonesian throughflow and remote forcing of the mixed layer-thermocline interactions and the
657 effect of biases in the windstress data used as a physical driver in the model.

658 Sensitivity experiments carried out by prescribing annual mean currents or temperatures over
659 selected subdomains reveal that the varZc retains the seasonality of carbon fluxes, pCO_2, and
660 export and new productions closer to observations. This strongly supports our contention that
661 varZc parameterization improves export and new productions and it is also efficient in capturing
662 upwelling episodes of the study regions. This points out the significant role of having a close
663 balance in seasonal biological export and new production in models to capture the seasonality in
664 carbon cycle. This also confirms the role of biological and solubility pumps in producing the
665 seasonality of carbon cycle in the upwelling zones.

However the underestimation of seasonality of CO_2 flux over the SLD and overestimation over the SC as well as the SCTR are a cautionary flag for the study. This uncertainty poses an important scientific question as to whether the model biology over the SC and SCTR region is not resolving the seasonality in CO_2 flux and pCO_2 properly or whether the seasonality in the compensation depth is not able to fully capture the biological processes.

To address these questions we have used an inverse modeling approach (Bayesian inversion) in order to optimize the spatially and temporally varying compensation depth using surface pCO_2 as the observational constraint and computed the optimized biological production. The results will be reported elsewhere.

Appendix - A

For Z <Zc,

$$J_{prod} = \frac{1}{\tau}([PO_4] - [PO_4^*]), \qquad [PO_4] > [PO_4^*] \tag{A1}$$

$$J_{DOP} = \sigma J_{prod} - \kappa[DOP] \tag{A2}$$

$$J_{PO4} = -J_{prod} + \kappa[DOP] \tag{A3}$$

$$J_{ca} = Rr_{C:P}(1-\sigma)J_{prod} \tag{A4}$$

$$J_{DIC} = r_{C:P}J_{PO4} + J_{ca} \tag{A5}$$

$$J_{ALK} = -r_{N:P}J_{PO4} + 2J_{ca} \tag{A6}$$

For Z >Zc,

$$J_{prod} = 0, \qquad [PO_4] \leq [PO_4^*] \tag{A7}$$

$$J_{DOP} = -\kappa[DOP] \tag{A8}$$

$$J_{PO4} = -\frac{\partial F}{\partial Z} + \kappa[DOP] \tag{A9}$$

$$F(Z) = F_c\left(\frac{Z}{Zc}\right)^{-a} \tag{A10}$$

$$F_c = (1-\sigma)\int_0^{Zc} J_{prod}\, dZ \tag{A11}$$

$$J_{ca} = -\frac{\partial F_{Ca}}{\partial Z} \tag{A12}$$

$$F_{Ca} = Rr_{C:P}F_C e^{-(z-Zc)/d} \tag{A13}$$

Where Z is the depth and Zc is the compensation depth in the model. J_{prod} , J_{DOP}, J_{PO4}, J_{Ca} are the biogeochemical sources and sinks. Within the compensation depth (Z_c), the biological production in the model J_{prod} is calculated using equation A1. $[PO_4]$ is the model phosphate concentration and $[PO_4^*]$ is observational phosphate. τ is the restoration timescale assumed to be 30 days. Whenever the model phosphate exceeds the observational phosphate, it allows production.The observational phosphate data were taken from the World Ocean Atlas (WOA; Garcia et al., 2014). During biological production, a fixed fraction (σJ_{prod}) of phosphate is converted into Dissolved Organic Phosphate (DOP) which is a source for J_{DOP} (equation A2) and remaining $-\kappa[DOP]$ is exported downward below the compensation depth, which is further remineralized into inorganic phosphate and made available for further biological production (equation A3). The downward flux of phosphate which is not converted into DOP within the compensation depth is given by equation A11. The decrease of flux with depth due to remineralization is shown by equation A10. The values of the constants a, κ, σ are 0.9, 0.2/year to 0.7/year, 0.67, respectively. The rate of production is used to explain the formation of calcium carbonate cycle in surface waters (equation A4) and its export is given by equation A12, where R is the rain ratio, a constant molar ratio of exported particulate organic carbon to the exported calcium carbonate flux at compensation depth. The exponential decrease of calcium carbonate flux with scale depth d is given by equation A13. The biological source or sink of dissolved inorganic carbon (DIC) and alkalinity (ALK) is explained through equations A5 and A6, respectively. Where the values of rain ratio (R) is taken as 0.07 and the Redfield ratio, $r_{C:P} = 106$, and $r_{N:P} = 16$ and scale depth d is chosen as 3500m.

Biological and Solubility Pump calculations

The biological effect on DIC is calculated from Louanchi et al., (1996). The tendency of DIC due to biomass production and calcite formation in the production zone is expressed as below.

$$\left(\frac{\partial DIC}{\partial t}\right)_b = \left(\frac{\partial PO_4}{\partial t}\right)_b \times R_{C:P} - J_{Ca} \qquad \text{(A14)}$$

The total tendency of DIC in the production zone is:

$$\left(\frac{\partial DIC}{\partial t}\right)_{total} = \left(\frac{\partial DIC}{\partial t}\right)_b + \int_x \int_y \Phi dx\, dy \qquad \text{(A15)}$$

where $\left(\frac{\partial DIC}{\partial t}\right)_b$ is the evolution of DIC due to the impact of biology (i.e., biological pump). The first term in the R.H.S of Equation A14 is the rate of change of phosphate which represents biological production in the model multiplied by the carbon to phosphorous Redfield ratio ($R_{C:P}$ = 117:1) and J_{Ca} represents the calcite formation in the model (see Equation A4 & A12). The solubility pump is calculated as the surface integral of the flux Φ (Louanchi et al., 1996).

Acknowledgement

The OCMIP-II routines were taken from (http://ocmip5.ipsl.jussieu.fr/OCMIP/). GFDL data for OTTM is taken from (http://data1.gfdl.noaa.gov/nomads/forms/assimilation.html).Takahashi data is taken from (http://www.ldeo.columbia.edu/res/pi/CO2/).The computations were carried out in High Performance Computing (HPC) of Ministry of Earth Sciences (MoES), IITM. Ms. Shikha Singh, Ms. Anju M (IITM) and Mr. Saran Rajendran (CUSAT) are thanked for initial helps and discussions.

760 **References**

761 Anderson, L. A., Sarminento, J. L.: Global ocean phosphate and oxygen simulations, Global
762 Biogeochem. Cycles, 9, 621-636, doi:10.1029/95GB01902, 1995.

763 Asselin, R.: Frequency filter for time integrations, Mon. Wea. Rev., 100, 487–490, doi:
764 10.1175/1520-0493, 1972.

765 Banse, K., McClain, C. R.: Winter blooms of phytoplankton in the Arabian Sea as observed by
766 the Coastal Zone Color Scanner, Mar. Ecol. Prog. Ser, 34, 201 – 211, 1986.

767 Banse, K.: Seasonality of phytoplankton chlorophyll in the central and northern Arabian Sea,
768 Deep Sea Res., 34, 713 – 723, doi:10.1016/0198-0149, 1987.

769 Barber, R. T., Marra. J., Bidigare. R. C., Codispoti. L. A., Halpern. D., Johnson. Z., Latasa. M.,
770 Goericke. R., and Smith. S. L.: Primary productivity and its regulation in the Arabian Sea during
771 1995, Deep. Sea. Res. pt. II, 48, 1127 – 1172. doi:10.1016/S0967-0645, 2001.

772 Bates, N. R., Pequignet. A. C., and Sabine. C. L.: Ocean carbon cycling in the Indian Ocean: 2.
773 Estimates of net community production, Global Biogeochem. Cycles., 20, GB3021,
774 doi:10.1029/2005GB002492, 2006.

775 Bauer, S., Hitchcock, G. L., Olson, D. B.: Influence of monsoonally-forced Ekman dynamics
776 upon surface-layer depth and plankton biomass distribution in the Arabian Sea, Deep Sea Res.,
777 38, 531 – 553, doi:10.1016/0198-0149, 1991.

778 Behrenfeld, M. J., Falkowski. P. G.: Photosynthetic rates derived from satellite-based
779 chlorophyll concentration, Limnol. Oceanogr., 42, 1 – 20, doi: 10.4319/lo.1997.42.1.0001, 1997.

780 Boyd, P. W., Rynearson, T. A., Armstrong, E. A., Fu. F., Hayashi. K. and co-authors.: Marine
781 Phytoplankton Temperature versus growth responses from polar to tropical waters – outcome of
782 a scientific community-wide study, PLoS ONE 8(5)., e63091,
783 Doi:10.1371/journal.phone.0063091, 2013.

784 Brock, J C., McClain, C. R.: Interannual variability of the southwest monsoon phytoplankton
785 bloom in the north-western Arabian Sea, J. geophys. Res., 97(C1), 733 – 750,
786 doi/10.1029/91JC02225, 1992.

787 Brock, J. C., McClain, C. R., Hay, W. W.: A southwest monsoon hydrographic climatology for
788 the northwestern Arabian Sea, J. geophys. Res., 97(C6), 9455 – 9465, doi: 10.1029/92JC00813,
789 1992.

790 Brock, J. C., McClain, C. R., Luther, M. E., Hay, W. W.: The phytoplankton bloom in the
791 northwestern Arabian Sea during the southwest monsoon of 1979, J. geophys. Res., 96(C11),
792 623 – 642, doi: 10.1029/91JC01711, 1991.

793 Brock. J., Sathyendranath. S., and Platt. T.: Modelling the seasonality of subsurface light and
794 primary production in the Arabian Sea, Mar. Eco. Prog. Ser., 101, 209 – 221, 1993.

795 Bruce, J. G.: Some details of upwelling off the Somali and Arabian coasts, J. mar. Res., 32, 419
796 – 423, 1974.

797 Bryan. K., Lewis, L. J.: A water mass model of the world ocean, J. Geophys. Res., 84, 2503 –
798 2517, doi: 10.1029/JC084iC05p02503, 1979.

799 Chang, Y. S., Zhang. S., Rosati. A., Delworth. T., Stern. W. F.: An assessment of oceanic
800 variability for 1960-2010 from the GFDL ensemble coupled data assimilation, Clim. Dyn., 40,
801 775 – 803, doi: 10.1007/s00382-012-1412-2, 2012.

802 Christian J. R., Verschall M. A., Murtugudde R., Busalacchi A. J., McClain C. R.:
803 Biogeochemical modelling of the tropical Pacific Ocean. II: Iron biogeochemistry, Deep Sea
804 Res., 49, 545 – 565, doi:10.1016/S0967-0645, 2001.

805 Colwell, R. R.: Global climate and infectious disease: the cholera paradigm, Science., 274(5295),
806 2025 – 2031, doi: 10.1126/science.274.5295.2025, 1996.

807 Dilmahamod A. F., Hermes. J. C., Reason C. J. C.: Chlorophyll-a variability in the Seychelles-
808 Chagos Thermocline Ridge: Analysis of a coupled biophysical model, J. of. Mar. Sys., 154, 220
809 – 232, doi:10.1016/j.jmarsys.2015.10.011, 2016.

810 Doney S. C., and co-authors.: Evaluating global ocean carbon models: The importance of
811 realistic physics, Glob. Biogeochem. Cycles, 18, doi:10.1029/2003GB002150, 2004.

812 Eppley, R. W., Peterson. B. J.: Particulate organic matter flux and planktonic new production in
813 the deep ocean, Nature, 282, 677-680, doi:10.1038/282677a0, 1979.

814 Eppley, R. W.: Temperature and phytoplankton growth in the sea, Fish. Bull., 70, 1063 – 1085,
815 1972.

816 Feely, R. A., Sabine, C. L., Takahashi, T., Wanninkhof, R.: Uptake and Storage of Carbon
817 Dioxide in the Ocean: The Global CO_2 Survey, Oceanography., 14(4), 18–32,
818 doi:10.5670/oceanog.2001.03, 2001.

819 Friedrichs, M. A. M., and co-authors.: Assessment of skill and portability in regional
820 biogeochemical models: role of multiple planktonic groups, J. GeoPhy. Res., 112, doi:
821 10.1029/2006JC003852, 2007.

822 Friedrichs, M. A. M., Hood, R. R., Wiggert, J. D.: Ecosystem complexity versus physical forcing
823 quantification of their relative impact with assimilated Arabian Sea data, Deep Sea Res., 53, 576-
824 600, doi:10.1016/j.dsr2.2006.01.026, 2006.

825 Garcia, H. E., R. A. Locarnini, T. P. Boyer, J. I. Antonov, O.K. Baranova, M.M. Zweng, J.R.
826 Reagan, D.R. Johnson.: World Ocean Atlas 2013, Volume 4: Dissolved Inorganic Nutrients
827 (phosphate, nitrate, silicate), S. Levitus, Ed., A. Mishonov Technical Ed.; NOAA Atlas NESDIS
828 76, 25 pp, 2014.

829 Gattuso, J. P., B. Gentili, C. M. Duarte, J. A. Kleypas, J. J. Middelburg, and D. Antoine.: Light
830 availability in the coastal ocean: Impact on the distribution of benthic photosynthetic organisms
831 and their contribution to primary production, Biogeosciences, 3, 489 – 513, doi:10.5194/bg-3-
832 489-2006, 2006.

833 Gent, P. R., McWilliams. J. C.: Isopycnal mixing in ocean circulation models, J. Phys.
834 Oceanogr., 20, 150 – 155, doi: 10.1175/15200485, 1990.

835 Harwell, C., Kim, K., Burkholder, J., Colwell, R., Epstein, P. R., Grimes, D., Hofmann, E. E.,
836 Lipp, E. K., Osterhaus, A., and Overshreet, R. M.: Emerging marine diseases-climate links and
837 anthropogenic factors, Science., 285(5433), 1505 – 1510, doi: 10.1126/science.285.5433.1505,
838 1999.

839 Howden, S., Murtugudde, R.: Effects of river inputs into the Bay of Bengal, J. Geophys. Res.,
840 106, 19,825-19,843. doi: 10.1029/2000JC000656, 2001.

841 Jerlov N. G.: Marine optics, Second ed., Elsevier, pp 231, 1976.

842 Jung, E., and Kirtman. B. P.: ENSO modulation of tropical Indian ocean subseasonal variability,
843 Geophy. Res. Lett., 43, doi: 10.1002/2016GL071899, 2016.

844 Keeling, C. D., Whorf, T. P., Wahlen, M., and van der plicht, J.: Interannual extremes in the rate
845 of rise of atmospheric carbon dioxide since 1980, Nature, 375, 666 – 670, 1995.

846 Key, R. M., et al,.: A global ocean carbon climatology: Results from Global Data Analysis
847 Project (GLODAP), Global Biogeochem. Cycles, 18, GB4031, doi:10.1029/2004GB002247,
848 2004

849 Krey, J., Bahenerd, B.: Phytoplankton production atlas of the international Indian Ocean
850 expedition, Institut fur Meereskundeander Universitat Kiel, Kiel, German, 1976.

851 Large, W. G., McWilliams, J. C., Doney, S. C.: Oceanic vertical mixing: A review and a model
852 with a nonlocal boundary layer parameterization, Rev. Geophys., 32, 363 – 403, doi:
853 10.1029/94RG01872, 1994.

854 Le Quere, C., Orr, J. C., Monfray, P., Aumont, O.: Interannual variability of the oceanic sink of
855 CO_2 from 1979 through 1997, Global Biogeochem. Cycles., 14, p1247 – 1265, doi:
856 10.1029/1999GB900049, 2000.

857 Lee, P. F., Chen, I. C., Tzeng. W. N.: Spatial and Temporal distributions patterns of bigeye tuna
858 (Thunnusobsesus) in the Indian Ocean, Zoological studies-Taipei-, 44(2), 260, 2005.

Lehodey .P., Senina I., Sibert. J., Bopp. L., Calmettes B., Hampton .J., Murtugudde. R.: Preliminary forecasts of Pacific bigeye tuna population trends under the A2 IPCC scenario, Prog in Oceanography., 86, 302 – 315, doi:10.1016/j.pocean.2010.04.021, 2010.

Liao, X., Zhan, H., Du, Y.: Potential new production in two upwelling regions of the Western Arabian Sea: Estimation and comparison, J. Geophy. Res. Oceans., 121, doi:10.1002/2016JC011707, 2016.

Louanchi. F., N. Metzl., and Alain Poisson.: Modelling the monthly sea surface f_{CO2} fields in the Indian Ocean, Marine Chemistry, 55, 265 – 279, 1996.

Lopez-Urrutia, A., E. San Martin, R. P. Harris, and X. Irigoien.: Scaling the metabolic balance of the oceans, Proc. Natl. Acad. Sci. U.S.A., 103, 8739-8744,doi:10.1073/pnas.0601137103, 2006.

Marra, J. F., Veronica P. Lance, Robert D. Vaillancourt, Bruce R. Hargreaves.: Resolving the ocean's euphotic zone, Deep Sea. Res. pt. I., 83, 45 -50, doi:10.1016/j.dsr.2013.09.005, 2014.

Matsumoto K., Tokos. K. S., Price., A. R., Cox. S. J.: First description of the Minnesota Earth System Model for Ocean biogeochemistry (MESMO 1.0), Geosci. Model Dev., 1, 1-15, doi:10.5194/gmd-1-1-2008, 2008.

McCreary, J., Murtugude, R., Vialard, J., Vinayachandran, P., Wiggert, J. D., Hood, R. R., Shankar, D., Shetye, S.: Biophysical processes in the Indian Ocean, Indian Ocean Biogeochemical Processes and Ecological Variability., 9 – 32, doi: 10.1029/GM185, 2009.

Moisan, J. R., Moisan, A. T., Abbott, M. R.: Modelling the effect of temperature on the maximum growth rates of phytoplankton populations, Eco. Modelling., 153, 197-215, doi:10.1016/S0304-3800(02)00008, 2002.

Morel, A.: Optical modeling of the upper ocean in relation to its biogenous matter content (Case 1 Waters), J. Geophys. Res., 93, 10479-10, 768, doi: 10.1029/JC093iC09p10749, 1988.

Murtugudde R., McCreary J. P., Busalacchi, A. J.: Oceanic processes associated with anomalous events in the Indian Ocean with relevance to 1997-1998, J. Geophy. Res., 105, 3295-3306, doi: 10.1029/1999JC900294, 2000.

Murtugudde, R., Busalacchi, A. J.: Interannual variability of the dynamics and thermodynamics of the tropical Indian Ocean, J. Clim. 12, 2300-2326, doi:10.1175/1520-0442, 1999.

Murtugudde, R., Seager, R., Thoppil, P.: Arabian Sea response to monsoon variations, Paleoceanography., 22, PA4217, doi:10.1029/2007PA001467, 2007.

Najjar, R. G., Keeling, R. F.: Analysis of the mean annual cycle of the dissolved oxygen anomaly in the world ocean, J. Mar. Res., 55, 117 – 151, doi:10.1357/0022240973224481, 1997.

Najjar, R. G., Orr, J. C.: Design of OCMIP-2 simulations of chlorofluorocarbons, the solubility pump and common biogeochemistry, http://www.ipsl.jussieu.fr/OCMIP/., 1998.

Najjar, R. G., Sarmiento, J. L., Toggweiler, J. R.: Downward transport and fate of organic matter in the ocean: simulations with a general circulation model, Global biogeochem. Cycles., 6, 45-76, doi/10.1029/91GB02718, 1992.

Naqvi, S. W. A., Moffett, J. W., Gauns, M. U., Narvekar, P. V., Pratihary, A. K., Naik, H., Shenoy, D. M., Jayakumar, D. A., Goepfert, T. J., Patra, P. K., Al-Azri, A., and Ahmed, S. I.: The Arabian Sea as a high-nutrient, low-chlorophyll region during the late Southwest Monsoon, Biogeosciences., 7, 2091-2100, doi:10.5194/bg-7-2091-2010, 2010.

900 Naqvi, S., Naik, H., Narvekar, P.: The Arabian Sea, in Biogeochemistry, edited by K. Black and
901 G. Shimmield, pp. 156 – 206, Blackwell, Oxford, 2003.

902 Orr, J. C. and co-authors.: Estimates of anthropogenic carbon uptake from four three-
903 dimensional global ocean models, Glob. Biogeochem. Cycles., 15, p43 – 60, doi:
904 10.1029/2000GB001273, 2001.

905 Orr, J. C., Aumont, O., Bopp, L., Calderia, K., Taylor, K., et. al.: Evaluation of seasonal air-sea
906 CO2 fluxes in the global carbon cycle models, International open Science conference (Paris, 7-
907 10 Jan. 2003), 2003.

908 Osawa, T., Julimantoro, S.: Study of fishery ground around Indonesia archipelago using remote
909 sensing data, International archives of the Photogrammetry, Remote sensing and spatial
910 information science., vol XXXVIII, part-8, 2010.

911 Parsons, T. R., Takahashi, M., Habgrave, B.: In Biological Oceanographic Processes, 3rd ed.,
912 330pp., Pergamon Press, New York, doi: 10.1002/iroh.19890740411, 1984.

913 Prasanna Kumar, .S., Muraleedharan, P. M., Prasad, T. G., Gauns, M., Ramaiah, N., de Souza, S.
914 N., Sardesai, S., Madhupratap, M.: Why is the Bay of Bengal less productive during summer
915 monsoon compared to the Arabian Sea?, Geophys. Res. Lett., 29(24), 2235,
916 doi:10.1029/2002GL016013, 2002.

917 Prasanna Kumar, S., Roshin, P. R., Narvekar, J., Dinesh Kumar, P., Vivekanandan, E.: What
918 drives the increased phytoplankton biomass in the Arabian Sea?, Current Science, 99(I), 101 –
919 106, 2010.

Prassana Kumar. S, Ramaiah. N, Gauns. M., Sarma V. V. S. S., Muraleedharan. P. M., RaghuKumar. S., Dileep Kumar., Madhupratap. M.: Physical forcing of biological productivity in the Northern Arabian Sea during the Northeast Monsoon, Deep Sea Res. Pt. II., 48, 1115-1126, doi:10.1016/S0967-0645(00)00133-8, 2001.

Praveen, V., Ajayamohan**,** R. S., Valsala**,** V., Sandeep, S.: Intensification of upwelling along Oman coast in a warming scenario, Geophys. Res. Lett., 43, doi:10.1002/2016GL069638, 2016.

Qasim, S. Z.: Biological productivity of the Indian Ocean, J. mar. Sci., 6, 122 – 137, 1977.

Qasim, S. Z.: Oceanography of Northern Arabian Sea, Deep Sea Res., 29(9A), 1041 – 1068, doi:10.1016/0198-0149(82)90027-9, 1982.

Redi, M.: Oceanic isopycnal mixing by coordinate rotation, J. Phys. Oceanogr., 12, 1154 – 1158, doi: 10.1175/1520-0485, 1982.

Regaudie-de-Gioux, A., and C. M. Duarte.: Compensation irradiance for planktonic community metabolism in the ocean, Global Biogeochem. Cycles, 24, GB4013, doi:10.1029/2009GB003639, 2010.

Roxy, M. K., Modi, A., Murtugudde, R., Valsala, V., Panickal, S., Prasanna Kumar, S., Ravichandran, M., Vichi, M., Levy, M.: A reduction in marine primary productivity driven by rapid warming over the tropical Indian Ocean, 43, 826 – 833, J. Geophy. Res. Letters., doi:10.1002/2015GL066979, 2015.

Ryther, J., Menzel, D.: On the production, composition, and distribution of organic matter in the Western Arabian Sea, Deep Sea Research and Oceanographic Abstracts., 12(2), 199 -209. doi:10.1016/0011-7471(65)90025-2, 1965.

941 Ryther, J.: Photosynthesis in the ocean as function of light Intensity, Limnol. Oceanogr., vol 1,
942 issue 1, doi: 10.4319/lo.1956.1.1.0061, 1956.

943 Sarma V. V. S. S.: Net plankton community production in the Arabian Sea based on O_2 mass
944 balance model, Glob. biogeochem. Cycles., 18, GB4001, doi:10.1029/2003GB002198, 2004.

945 Sarma, V. V. S. S.: An evaluation of physical and biogeochemical processes regulating the
946 perennial suboxic conditions in the water column of the Arabian Sea, Global Biogeochem.
947 Cycles., 16, doi:10.1029/2001GB001461, 2002.

948 Sarmiento, J. L., and Gruber, N.: Ocean Biogeochemical Dynamics, Princeton University Press,
949 New Jersey, 2006.

950 Sarmiento, J. L., Monfray. P., Maier-Reimer., Aumont, O., Murnane, R. J., Orr, J. C.: Sea-air
951 CO_2 fluxes and carbon transport: A comparison of three ocean general circulation models,
952 Global Biogeochem. Cycles., 14, p1267 – 1281. doi: 10.1029/1999GB900062, 2000.

953 Schott, F.: Monsoon response of the Somali current and associated upwelling, Prog.Oceanogr.,
954 12, 357 – 381, doi:10.1016/0079-6611(83)90014-9, 1983.

955 Smetacek, V., and Passow, U.: Spring bloom initiation and Sverdrup's critical depth model,
956 Limnol. Oceanogr., 35, 228 – 234, doi: 10.4319/lo.1990.35.1.0228, 1990.

957 Smith, L. S.: Understanding the Arabian Sea: Reflections on the 1994-1996 Arabian Sea
958 Expedition, Deep Sea Res. Pt. II., 48, 1385-1402, doi:10.1016/S0967-0645(00)00144-2, 2001.

959 Smith, R. L., Bottero, L. S.: On upwelling in the Arabian Sea. In Angel, M (ed) A voyage of
960 Discovery. Pergammon Press, New York, p. 291 – 304, 1977.

961 Smith, S. L., Codistpoti, L. A.: Southwest monsoon of 1979: chemical and biological response of
962 Somali coastal waters. Science, 209, 597 – 600. doi:10.1126/science.209.4456.597, 1980.

963 Smith, S. L.: Biological indications of active upwelling in the northwestern Indian Ocean in 1964
964 and 1979, a comparison with peru and northwest Africa, Deep Sea Res., 31, 951 – 967,
965 doi:10.1016/0198-0149(84)90050-5, 1984.

966 Susanto. R., Gordon, A. L., Zheng. Q.: Upwelling along the coasts of Java and Sumatra and its
967 relation to ENSO, J. Geophy. Res. Lett., 28, 1599-1602, doi: 10.1029/2000GL011844, 2001.

968 Swallow, J. C.: Some aspects of the physical oceanography of the Indian Ocean, Deep Sea Res.,
969 31, 639 – 650, doi:10.1016/0198-0149(84)90032-3, 1984.

970 Takahashi, T., Sutherland, S. C., Wanninkhof, R., Sweeney, C., Feely, R. A., Chipman, D. W.,
971 Hales, B., Friederich, G., Chavez, F., Sabine, C., et al.: Climatological mean and decadal
972 changes in surface ocean pCO_2 and net sea-air CO_2 flux over the global oceans. Deep Sea Res.,
973 Pt. II., 56, 554 – 557, doi:10.1016/j.dsr2.2008.12.009, 2009.

974 Valsala, V.: Different spreading of Somali and Arabian coastal upwelled waters in the northern
975 Indian Ocean: A case study. J. Phy. Oceanogr., 803 – 816, doi: https://doi.org/10.1007/s10872-
976 009-0067-z, 2009.

977 Valsala V., Maksyutov, S.: A short surface pathway of the subsurface Indonesian Throughflow
978 water from the Java Coast associated with upwelling, Ekman Transport, and Subduction. Int. J.
979 Oceanogr., 15, doi: 10.1155/2010/540743, 2010.

980 Valsala V., Maksyutov, S.: Interannual variability of air-sea CO_2 flux in the north Indian Ocean,
981 Ocean Dynamics., 1 – 14, doi 10.1007/s10236-012-0588-7, 2013.

Valsala, K. V., Maksyutov, S., Ikeda, M.: Design and Validation of an offline oceanic tracer transport model for a carbon cycle study, J. clim., 21, doi: 10.1175/2007JCLI2018.1, 2008.

Valsala, V.**,** Maksyutov, S., Murtugudde, R.: Interannual to Interdecadal Variabilities of the Indonesian Throughflow Source Water Pathways in the Pacific Ocean, J. Phys. Oceanogr., 41, 1921–1940, doi: 10.1175/2011JPO4561.1, 2011.

Valsala, V., Maksyutov, S.: Simulation and assimilation of global **oc**ean pCO_2 and air-sea CO_2 fluxes using ship observations of surface ocean pCO_2 in a simplified biogeochemical model, Tellus., 62B, doi: 10.1111/j.1600-0889.2010.00495, 2010.

Valsala, V**.,** Murtugudde, R.: Mesoscale and Intraseasonal Air-Sea CO_2 Exchanges in the Western Arabian Sea during Boreal Summer, Deep Sea Res. Pt. I, 103, 103-113, doi:10.1016/j.dsr.2015.06.001, 2015.

Valsala, V.**,** Roxy, M., Ashok, K., Murtugudde, R.: Spatio-temporal characteristics of seasonal to multidecadal variability of pCO_2 and air-sea CO_2 fluxes in the equatorial Pacific Ocean, J. Geophys. Res., 119, 8987 – 9012, doi:10.1002/2014JC010212, 2014.

Vialard,. J. P. and co-authors.: Air-Sea Interactions in the Seychelles-Chagos Thermocline Ridge Region, BAMS, doi:10.1175/2008BAMS2499.1, 2009.

Vinayachandran P. N., Shankar D., S. Vernekar, K. K. Sandeep, P. Amol, C. P. Neema and A. Chatterjee.: A summer monsoon pump to keep the bay of Bengal salty, Geophys. Res. Lett., 40, 1777 – 1782, doi:10.1002/grl.50274, 2013.

1001 Vinayachandran P. N., Yamagata, T.: Monsoon Response of the Sea around Sri Lanka:
1002 Generation of Thermal Domes and Anticyclonic Vortices, J. Phy. Oceano., 28, 1946 – 1960, doi:
1003 10.1175/1520-0485, 1998.

1004 Vinayachandran, P. N., Chauhan, P., Mohan, M., Nayak, S.: Biological response of the sea
1005 around Sri Lanka to summer monsoon, Geophys. Res. Lett., 31, L0I302,
1006 doi:10.1029/2003GL018533, 2004.

1007 Wang .X. J., Behrenfeld. M., Le Borgne .R., Murtugudde .R., and Boss. E.: Regulation of
1008 phytoplankton carbon to chlorophyll ratio by light, nutrients and temperature in the equatorial
1009 Pacific Ocean: a basin-scale model. Biogeosciences., 6, 391 – 404, doi:10.5194/bg-6-391-2009,
1010 2009.

1011 Wiggert J. D., Jones. B. H., Dickey .T D., Brink .K. H., Weller .R .A., Marra. J., Codispoti. L.
1012 A.: The Northeast Monsoon's impact on mixing, phytoplankton biomass and nutrient cycling in
1013 the Arabian Sea, Deep Sea Res. Pt. II, 47, 1353-1385, doi:10.1016/S0967-0645(99)00147-2,
1014 2000.

1015 Wiggert, J. D., Hood, R. R., Banse, K., Kindle, J. C.: Monsoon-driven biogeochemical processes
1016 in the Arabian Sea, Progr. Oceanogr., 65, 176-213, doi:10.1016/j.pocean.2005.03.008, 2005.

1017 Wiggert. J. D., Murtugudde, R. G., Christian J. R.: Annual ecosystem variability in the tropical
1018 Indian Ocean: results of a coupled bio-physical ocean general circulation model, Deep Sea Res.
1019 Pt. II., 53, 644-676, doi:10.1016/j.dsr2.2006.01.027, 2006.

1020 Xie, S. P., Annamalai, H., Schott, F. A., McCreary Jr. J. P.: Structure and mechanism of south
1021 Indian ocean climate variability, J. clim., 15, 864 – 878, doi: 10.1175/1520-0442, 2002.

1022 Xing W., Xiaomei. L., Haigang Z., Hailong. L.: Estimates of potential new production in the
1023 Java-Sumatra upwelling system, Chinese Journal of Oceanology and Limnology., 30, 1063-
1024 1067, doi:10.1007/s00343-012-1281, 2012.

1025 Yamanaka, Y., Yoshie, N, MasahikoFujii, Maka .N. Aita and Kishi. M. J.: An Ecosystem
1026 coupled with Nitrogen-Silicon-Carbon cycles applied to station A7 in the Northwestern Pacific,
1027 J. of Oceanogr., 60, p227-241, doi: 10.1023/B:JOCE.0000038329.91976.7d, 2004.

1028 Zhou X., Weng. E., Luo., Y.: Modelling patterns of nonlinearity in the ecosystem responses to
1029 temperature, CO_2 and precipitation changes, Eco. Appli., 18, 453 – 466, doi: 10.1890/07-0626.1,
1030 2008.

1031

Table: 1 WAS = Western Arabian Sea, SLD = Sri Lanka Dome, SC = Sumatra Coast, SCTR = Seychelles-Chagos Thermocline Ridge. JJAS mean and climatological annual mean of CO_2 flux from Takahashi observations, constZc and varZc simulations. Units are mol m^{-2} yr^{-1}.

Regions	CO_2 flux (mol m^{-2} yr^{-1})					
	JJAS Mean			Annual Mean		
	OBS	constZc	varZc	OBS	constZc	varZc
WAS	1.99	1.44 ± 0.2	2.31 ± 0.4	0.94	0.80 ± 0.1	1.07 ± 0.2
SLD	1.79	-0.008 ± 0.2	0.24 ± 0.09	0.80	-0.02 ± 0.1	0.10 ± 0.2
SC	0.31	0.60 ± 0.5	1.51 ± 1.01	0.21	0.21 ± 0.3	0.53 ± 0.5
SCTR	0.82	-0.32 ± 0.3	-0.05 ± 0.4	0.55	-0.02 ± 0.1	-0.07 ± 0.2

Table: 2 Same as Table 1, but for pCO_2. Units are µatm.

Regions	pCO_2 (µatm)					
	JJAS Mean			Annual Mean		
	OBS	constZc	varZc	OBS	constZc	varZc
WAS	397.58	389.18 ± 3.7	399.95 ± 5.01	394.69	389.62 ± 3.9	391.19 ± 4.7
SLD	382.44	371.67 ± 6.04	379.24 ± 8.9	380.21	370.76 ± 6.1	374.94 ± 9.6
SC	372.52	382.36 ± 12.7	402.14 ± 21.8	372.69	374.65 ± 9.3	381.76 ± 13.6
SCTR	377.18	365.71 ± 5.08	370.72 ± 7.4	379.89	372.69 ± 4.7	369.00 ± 5.4

Table: 3 JJAS mean and climatological annual mean of export production from satellite derived Net Primary Production data, constZc and varZc simulations. Units are g C m^{-2} yr^{-1}.

Regions	Export Production (g C m^{-2} yr^{-1})					
	JJAS Mean			Annual Mean		
	OBS	constZc	varZc	OBS	constZc	varZc
WAS	123.57	84.81 ± 16.04	147.19 ± 23.8	94.31	77.41 ± 15.1	122.54 ± 25.2
SLD	51.54	167.71 ± 59.04	151.51 ± 46.4	43.25	144.43 ± 49.8	156.08 ± 43.8
SC	58.87	260.11 ± 104.7	310.03 ± 99.5	54.53	172.52 ± 72.4	215.52 ± 70.8
SCTR	51.08	57.39 ± 14.2	99.23 ± 21.8	40.45	55.15 ± 17.9	80.35 ± 26.04

Table: 4 Same as Table 3, but for New production.

Regions	New Production (g C m^{-2} yr^{-1})					
	JJAS Mean			Annual Mean		
	OBS	constZc	varZc	OBS	constZc	varZc
WAS	--	150.84 ± 27.9	133.03 ± 19.5	--	108.43 ± 23.4	81.47 ± 15.7
SLD	--	141.93 ± 64.1	77.78 ± 27.6	--	111.05 ± 71.1	50.37 ± 26.3
SC	--	63.64 ± 30.9	78.11 ± 29.1	--	56.69 ± 43.3	54.58 ± 23.3
SCTR	--	12.17 ± 16.3	13.32 ± 18.6	--	13.74 ± 15.5	12.94 ± 13

Table 5: Biological pump impact over DIC in the model due to constZc and varZc simulations for JJAS and annual mean.

Biological Pump ($gC\ m^{-2}\ yr^{-1}$)	**constZc**		**varZc**	
	JJAS Mean	**Annual Mean**	**JJAS Mean**	**Annual Mean**
WAS	45.18 ± 14.8	45.49 ± 14.38	151.7 ± 23.8	126.67 ± 24.3
SLD	89.39 ± 58.1	108.65 ± 48.6	156.07 ± 48.4	161.15 ± 43.5
SC	235.54 ± 95.4	155.21 ± 67.4	319.16 ± 94.9	222.92 ± 68.7
SCTR	30.49 ± 13.4	26.81 ± 16.8	103.13 ± 19.6	83.98 ± 23.6

Table 6: Same as Table 5, But for Solubility pump.

Solubility Pump ($gC\ m^{-2}\ yr^{-1}$)	**constZc**		**varZc**	
	JJAS Mean	**Annual Mean**	**JJAS Mean**	**Annual Mean**
WAS	17.29 ± 3.5	9.63 ± 2.1	27.72 ± 4.8	12.92 ± 2.7
SLD	-0.09 ± 2.4	-0.32 ± 2.3	2.9 ± 3.5	1.31 ± 3.5
SC	7.22 ± 6.9	2.56 ± 3.8	18.17 ± 12.1	6.43 ± 6.0
SCTR	-3.95 ± 3.7	-0.35 ± 2.3	-0.61 ± 5.3	-0.86 ± 2.8

Table 7: JJAS mean and climatological annual mean response from the model forced with annual mean currents.

WAS region forced with Annual mean currents	JJAS mean		Improvement	Climatological annual mean		Improvement
	constZc	varZc		constZc	varZc	
CO_2 flux (mol m^{-2} yr^{-1})	0.80 ± 0.2	1.29 ± 0.2	0.48 ± 0.04	0.65 ± 0.1	0.79 ± 0.1	0.13 ± 0.02
pCO_2 (µatm)	381.81 ± 3.4	387.24 ± 3.9	5.43 ± 0.5	388.68 ± 3.4	388.40 ± 3.6	-0.28 ± 0.1
Export production (g C m^{-2} yr^{-1})	60.71 ± 4.7	104.22 ± 13.4	43.51 ± 8.6	74.30 ± 4.5	104.58 ± 18.3	30.28 ± 13.7
New Production (g C m^{-2} yr^{-1})	34.76 ± 2.3	52.16 ± 1.51	17.39 ± 0.8	29.91 ± 1.7	44.72 ± 1.6	14.81 ± 0.1

Table 8 Same as Table 7 but from annual mean temperature simulation.

WAS region forced with Annual mean temperature	JJAS mean		Improvement	Climatological annual mean		Improvement
	constZc	varZc		constZc	varZc	
CO_2 flux (mol m^{-2} yr^{-1})	1.85 ± 0.2	2.74 ± 0.4	0.88 ± 0.1	0.81 ± 0.1	1.10 ± 0.2	0.28 ± 0.07
pCO_2 (µatm)	393.20 ± 3.01	404.26 ± 4.9	11.05 ± 1.9	384.61 ± 3.3	386.52 ± 4.8	1.91 ± 1.4

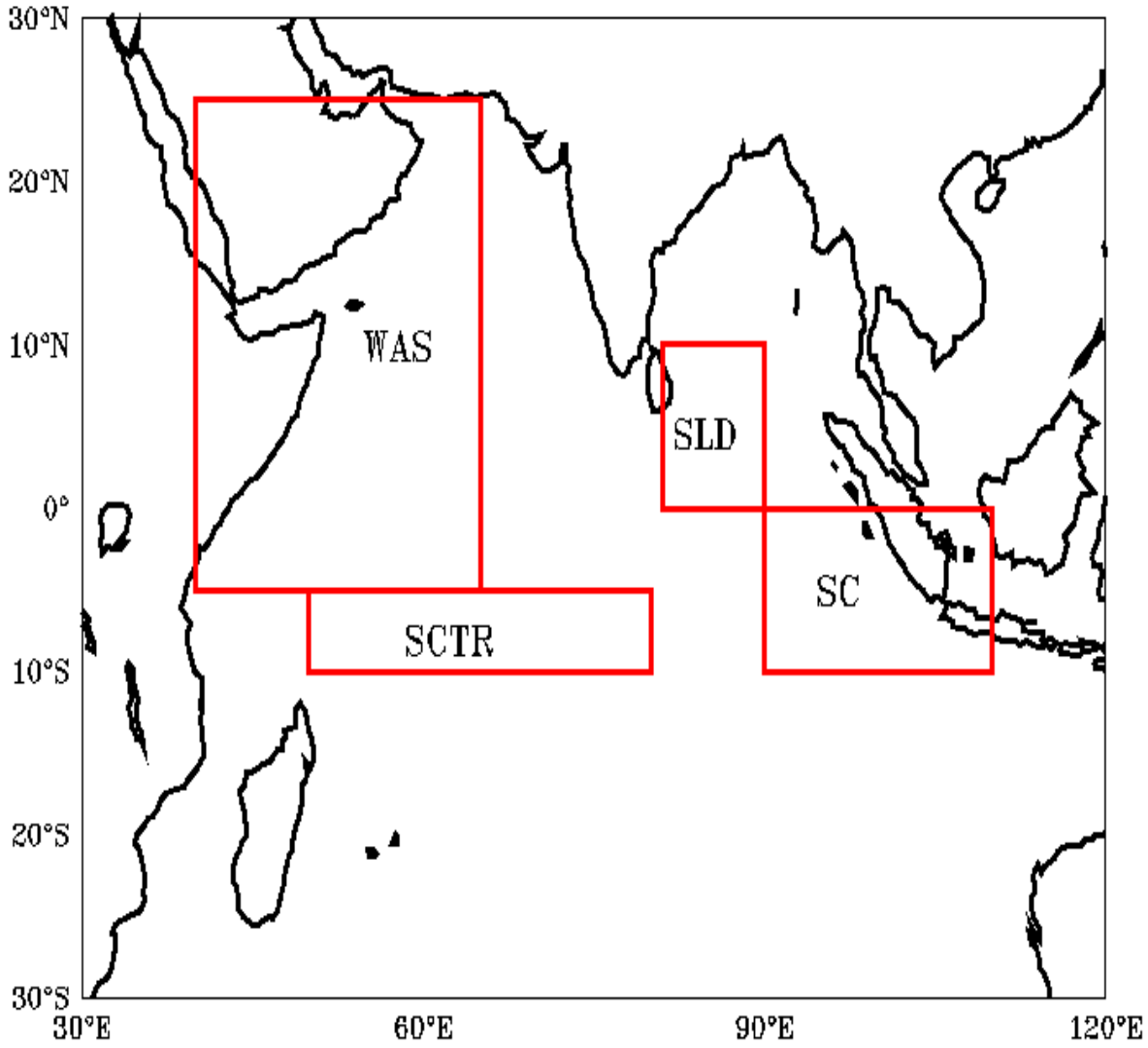

Figure 1: Red boxes shows the study regions (1) WAS (Western Arabian Sea, 40^{o}E:65^{o}E, 5^{o}S:25^{o}N) (2) SLD (Sri Lanka Dome, 81^{o}E:90^{o}E, 0^{o}:10^{o}N) (3) SCTR (Seychelles-Chagos Thermocline Ridge, 50^{o}E:80^{o}E, 5^{o}S:10^{o}S) and (4) SC (Sumatra Coast, 90^{o}E:110^{o}E, 0^{o}:10^{o}S).

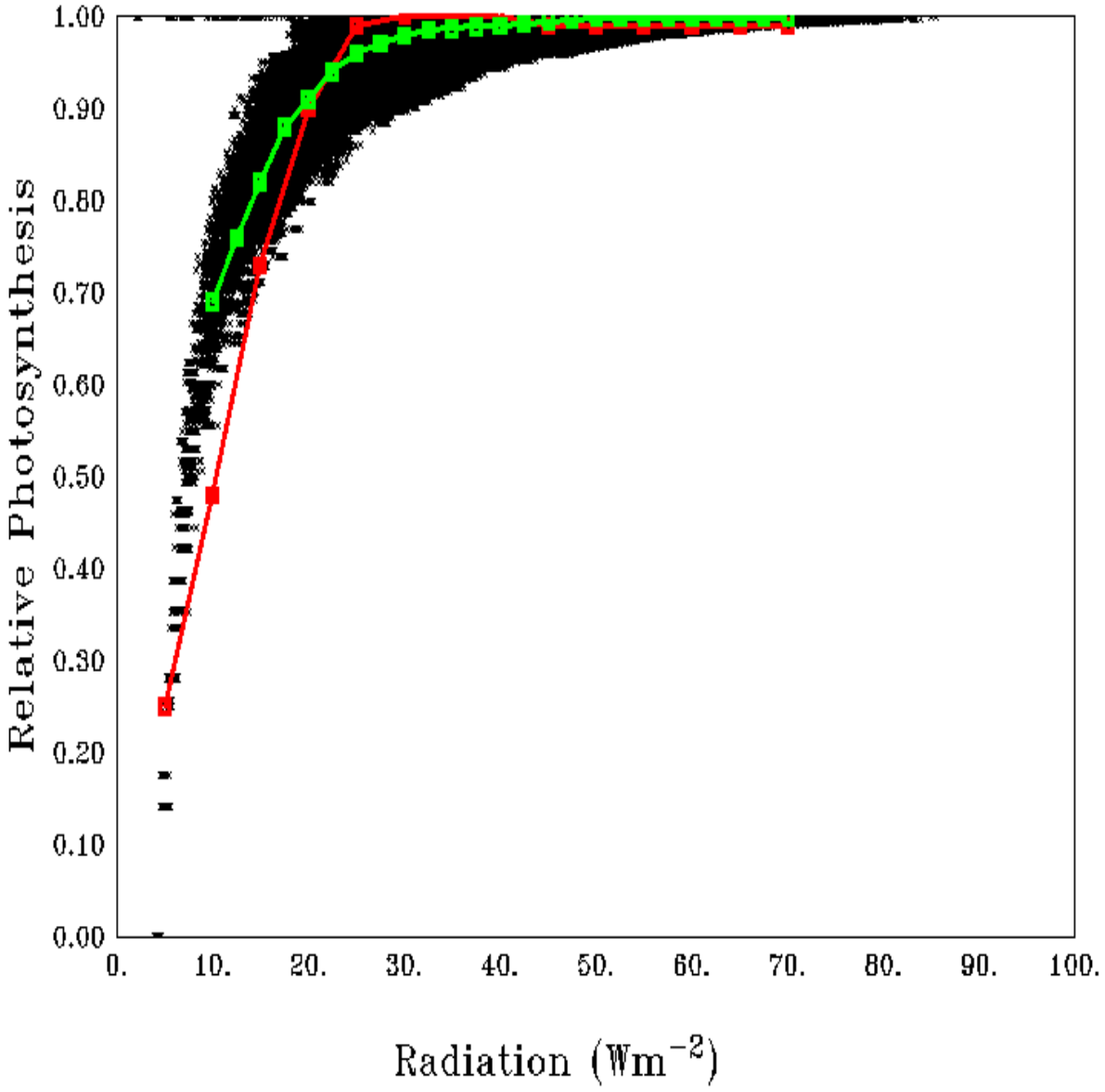

Figure 2: Scatter of average relative photosynthesis versus different light intensities in the model (black dots) and its mean (green curve). Red curve shows the theoretical P – I curve from Parsons et al., (1984).

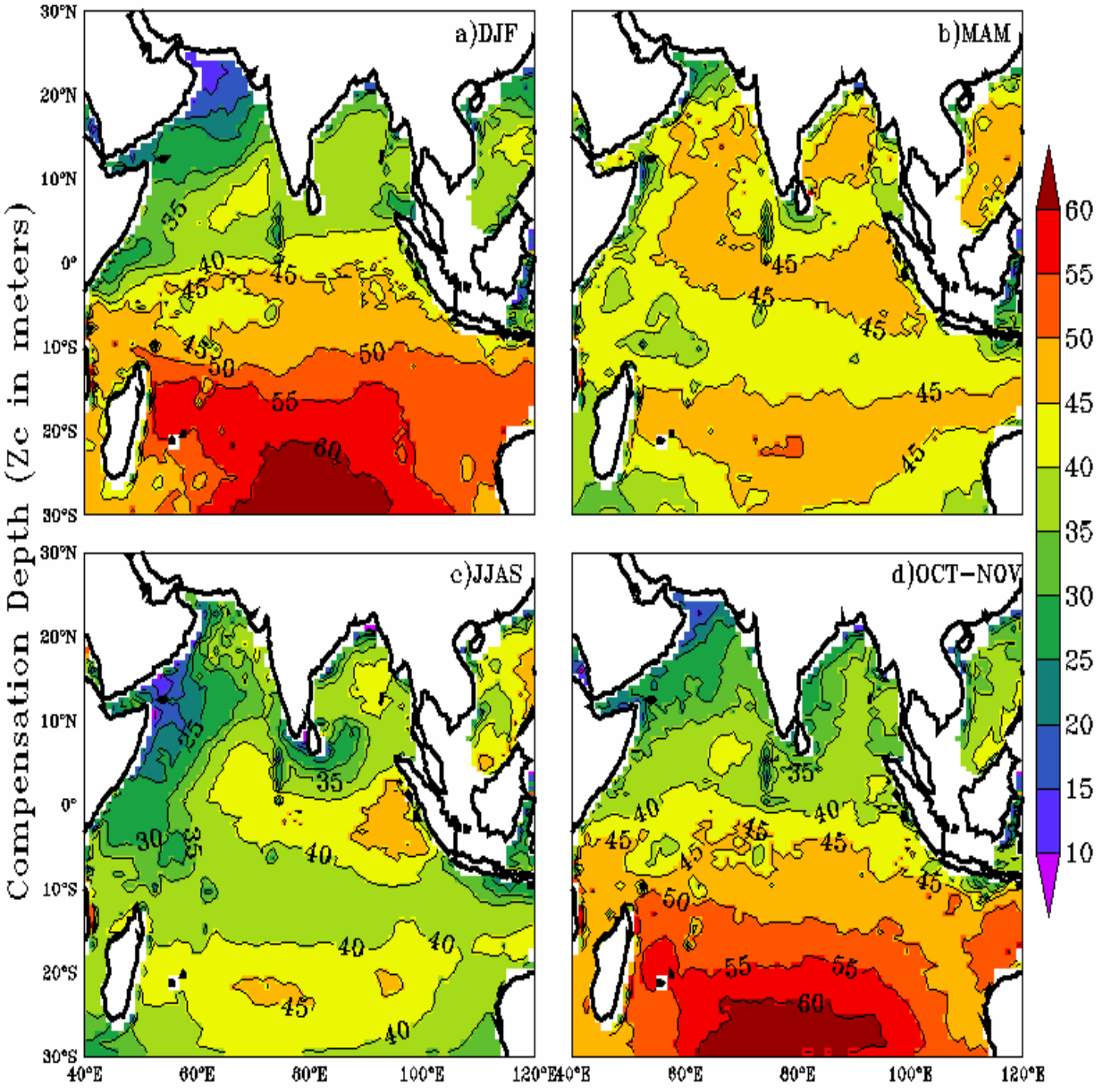

Figure 3: Seasonal mean maps of varying compensation depth (varZc), (a) December to February (DJF), (b) March to May (MAM), (c) June to September (JJAS), (d) October to November (OCT-NOV). Units are meters.

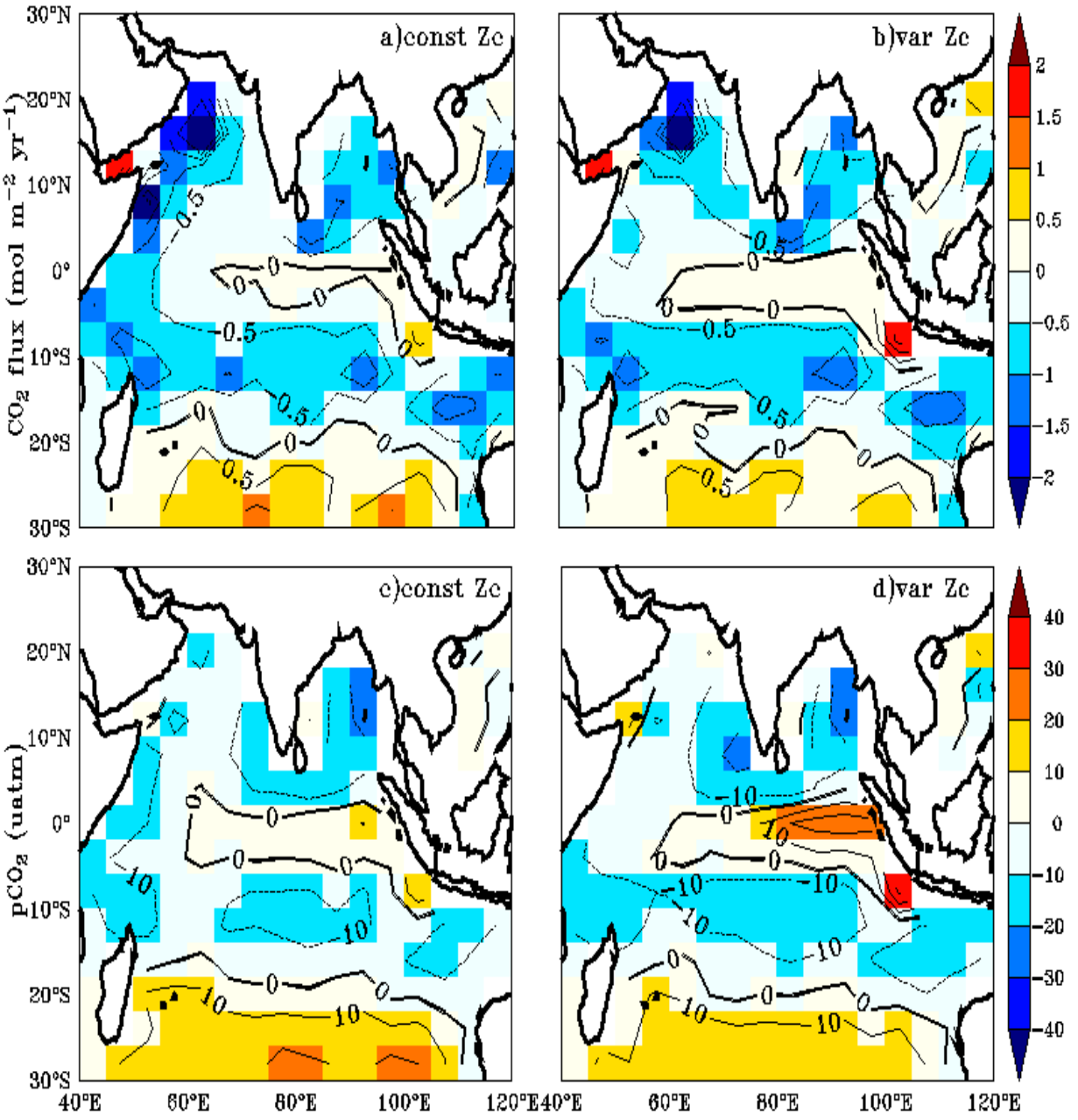

Figure 4: Annual mean biases in the model evaluated against Takahashi et al. (2009) observations for CO_2 flux (a, b) and pCO_2 (c, d) with constant Zc (constZc) and varying Zc (varZc). Units of CO_2 flux and pCO_2 are mol m^{-2} yr^{-1} and μatm, respectively.

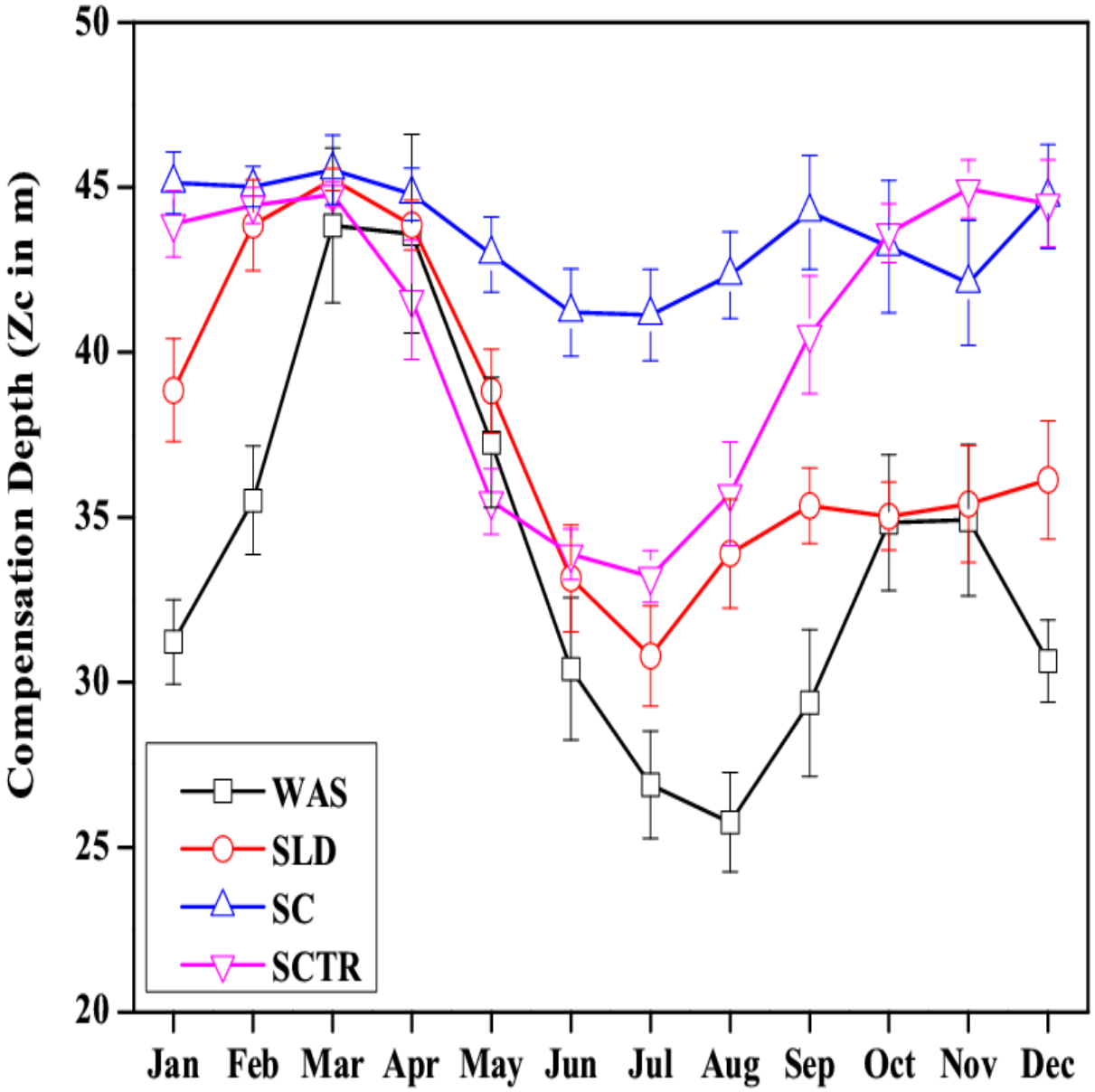

Figure 5: Seasonal variations in varZc over the study regions shown as climatology computed over 1990-2010. Error bar shows standard deviations of individual months over these years. Units are meters.

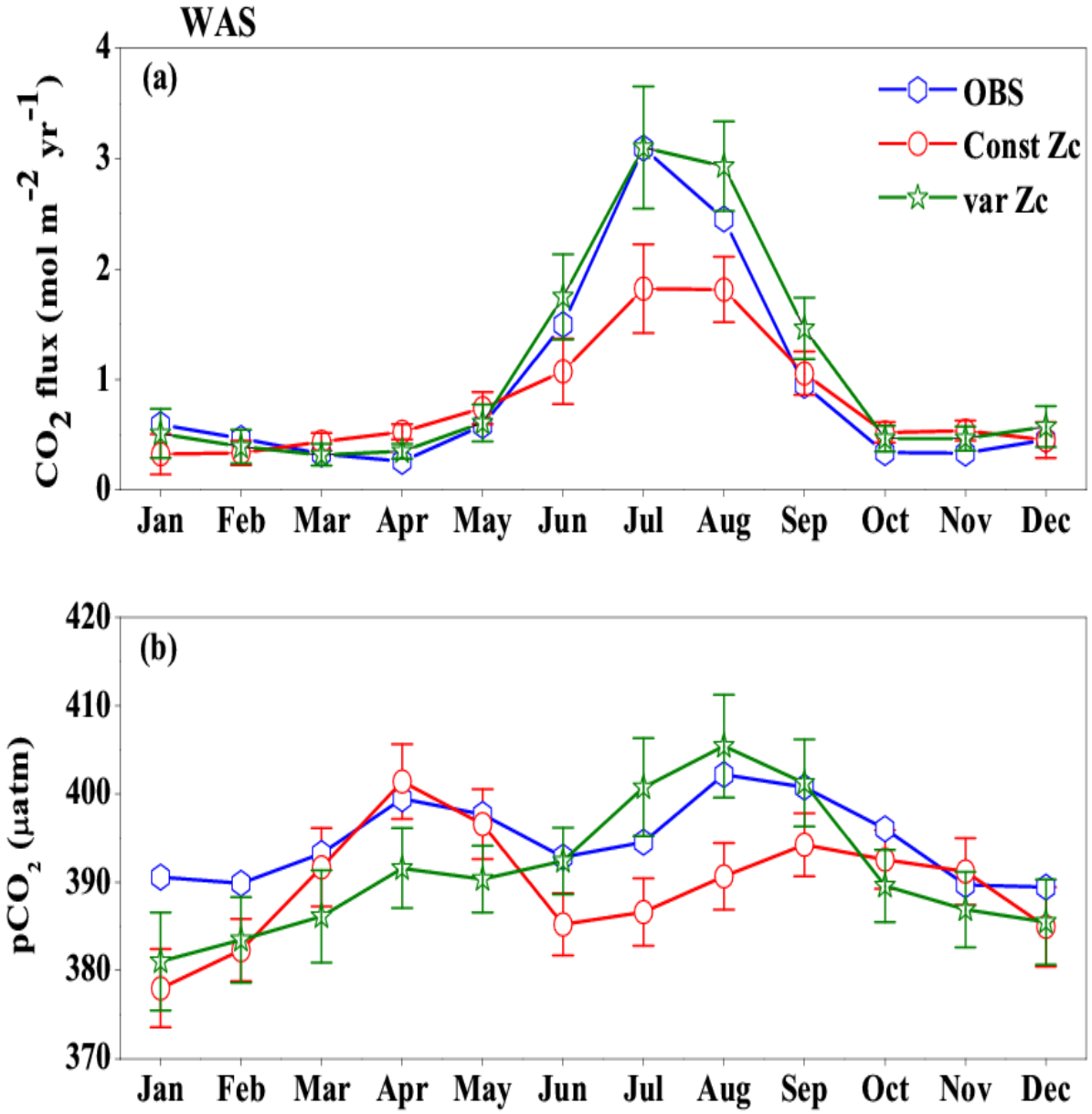

Figure 6: Comparison of model (a) CO_2 flux and (b) pCO_2 simulated with constZc and varZc with that of Takahashi et al. (2009) observations (OBS) over WAS as climatology computed over 1990-2010. Error bar shows standard deviations of individual months over these years. Units of CO_2 flux and pCO_2 are mol m^{-2} yr^{-1} and µatm, respectively. Legend is common for both graphs.

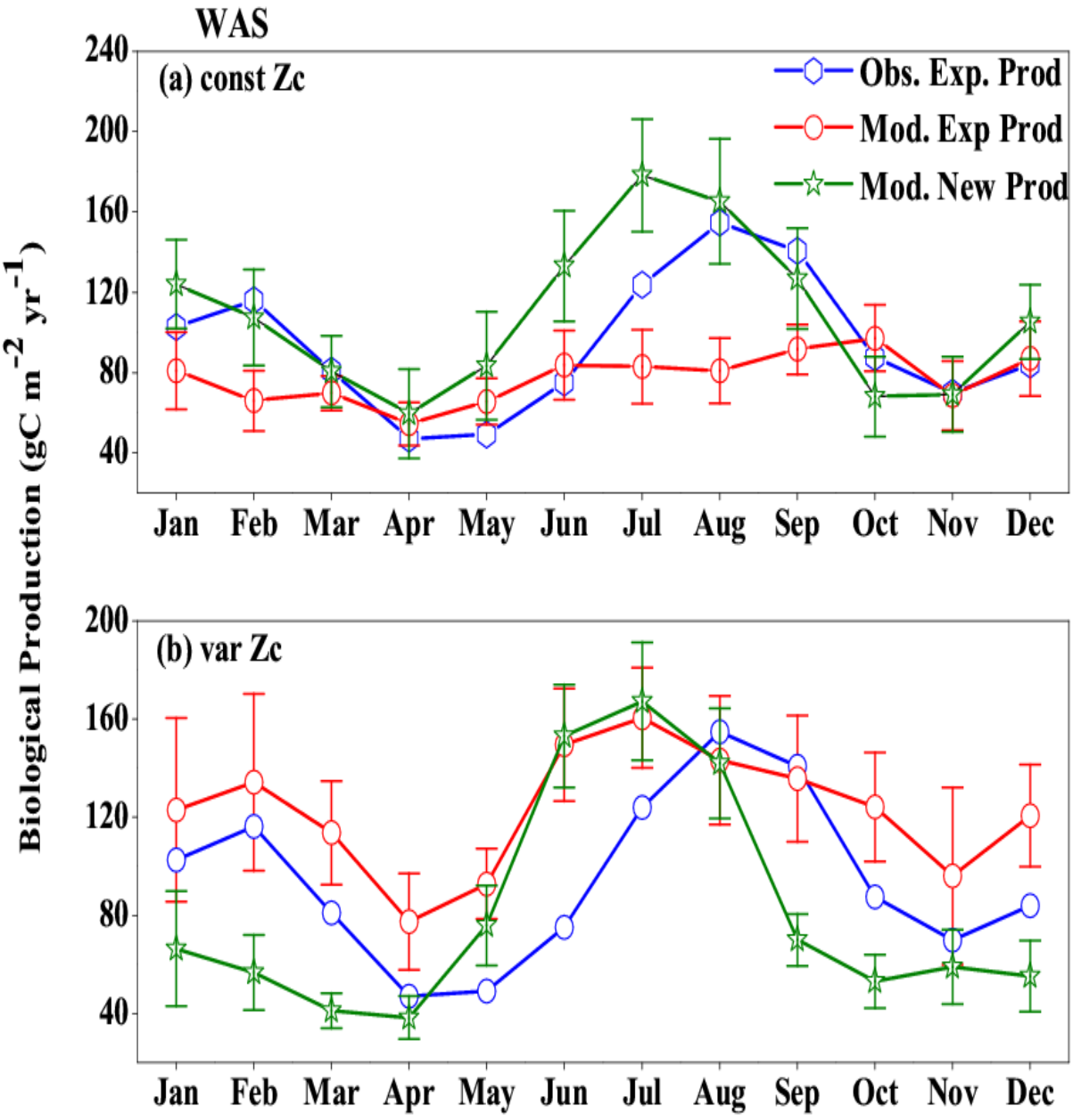

Figure 7: Comparison of model export production (Mod. Exp. Prod) and new production (Mod. New Prod) with satellite derived export production (Obs. Exp. Prod) for (a) ConstZc and (b) varZc simulations for WAS. Units are g C m^{-2} yr^{-1}. Legends are common for both graphs.

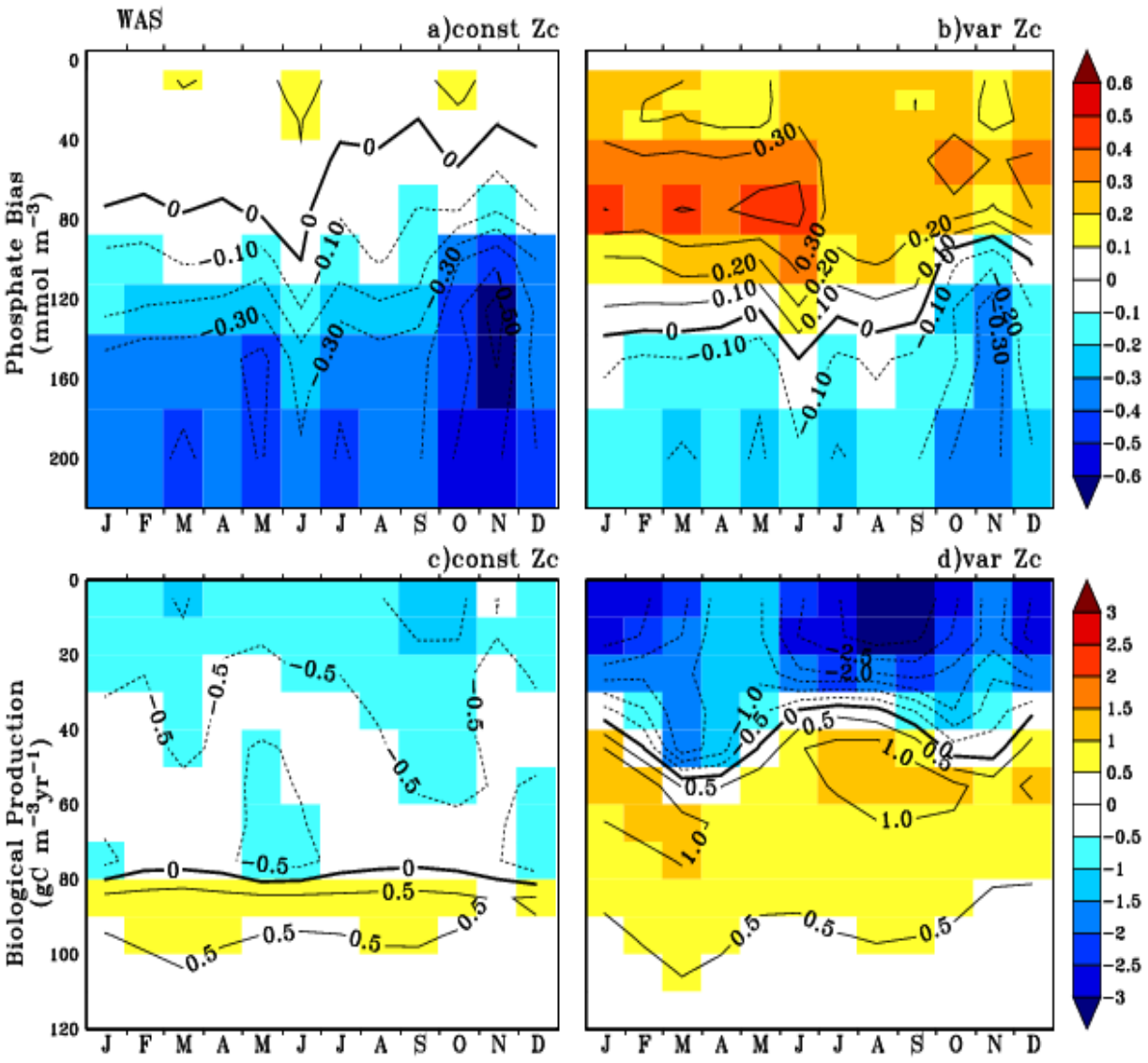

Figure 8: Annual mean bias of model phosphate when compared with climatological observational data (a) for constZc and (b) for varZc simulations. Corresponding annual mean biological source/sink profiles (c, d) in the model for WAS. Unit of phosphate is mmol m^{-3} and biological production is g C m^{-3} yr^{-1}.

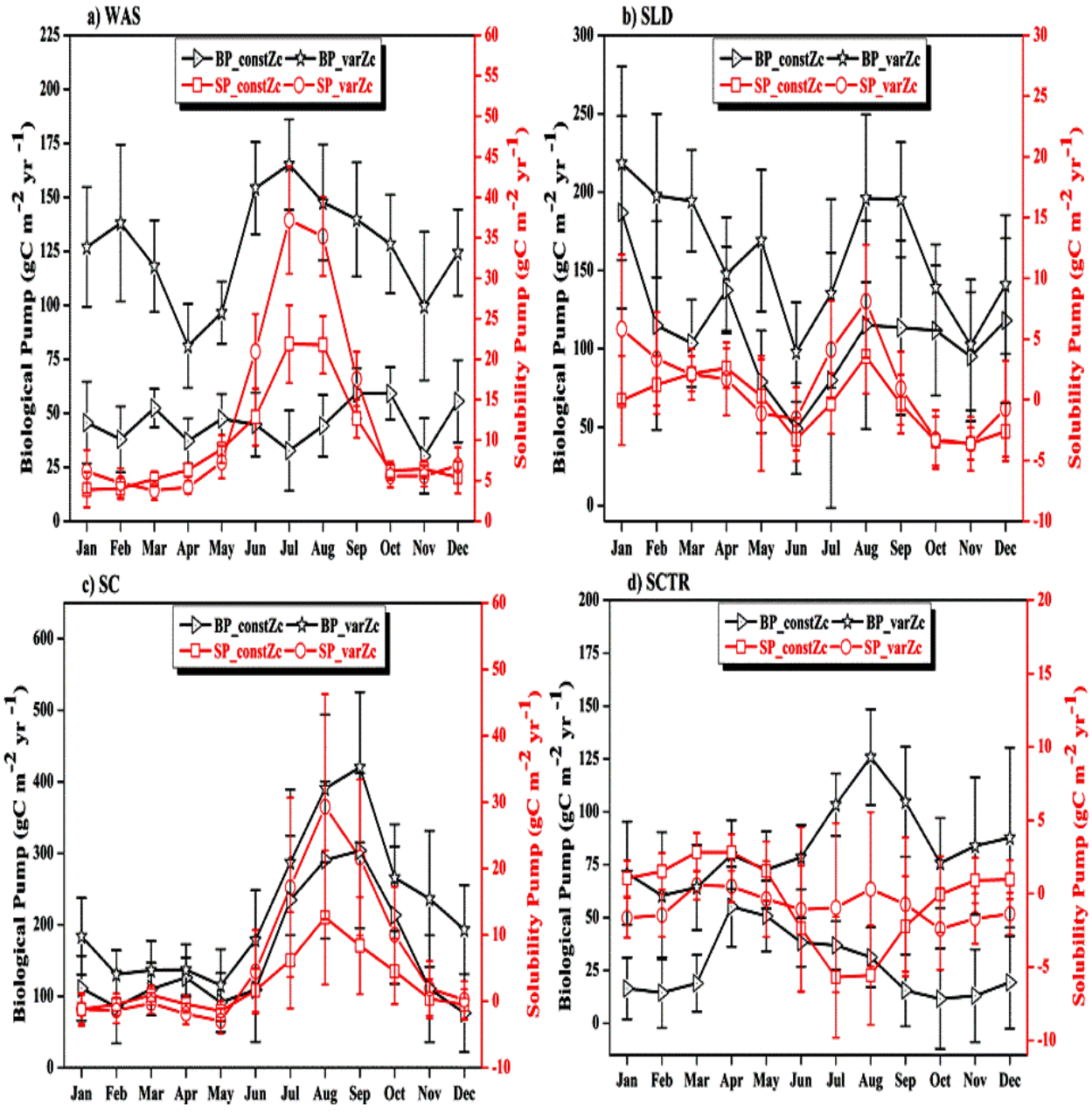

Figure 9: The strength of the biological pump (BP, black lines) and solubility pump (SP, red lines) from constZc and varZc simulations for (a) WAS (b) SLD (c) SC and (d) SCTR. The left axis shows the biological pump and the right axis shows the solubility pump. Error bar shows standard deviations of individual months over the years 1990 - 2010. Units are g C m^{-2} yr^{-1}.

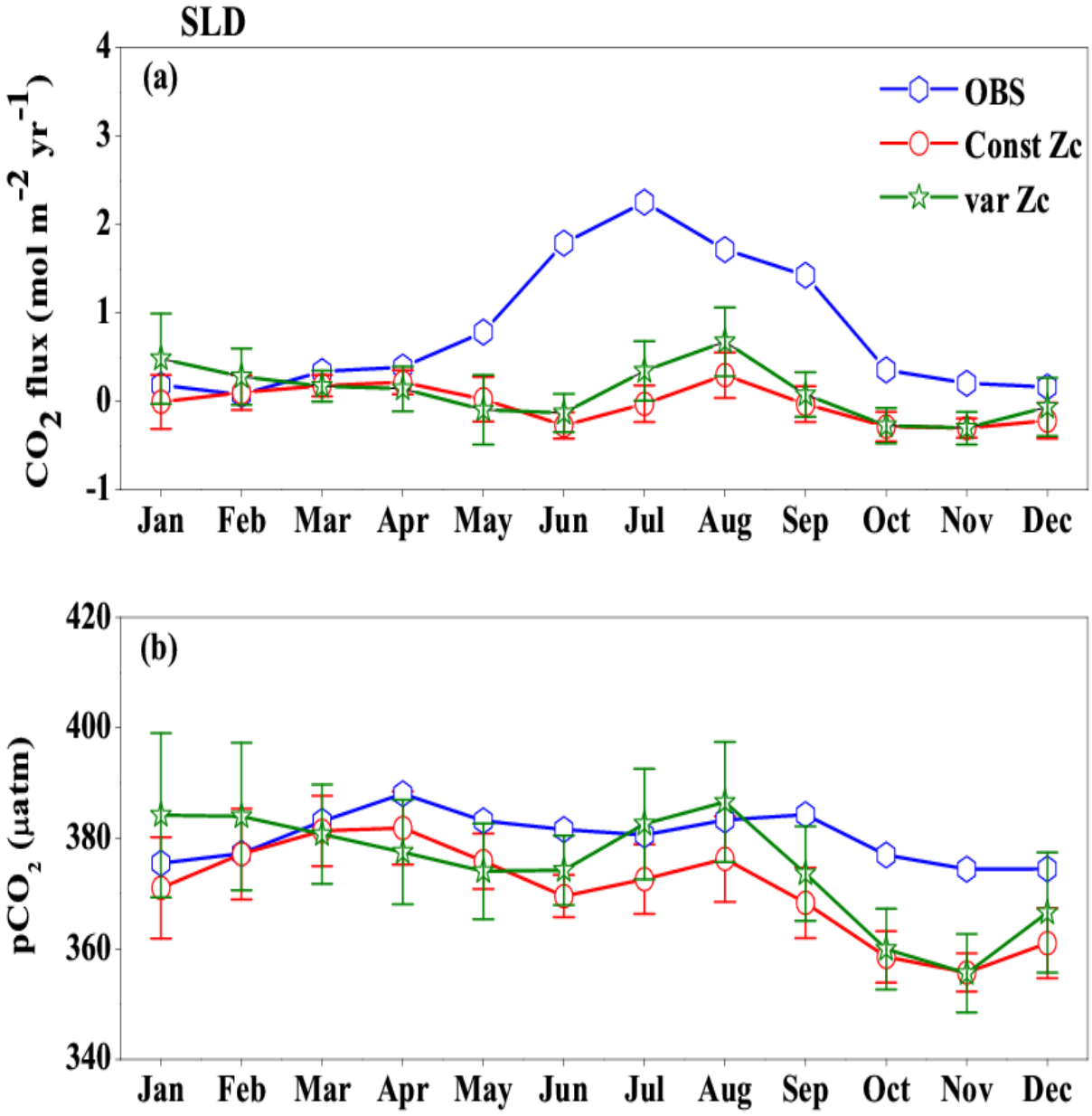

Figure 10: Same as Figure (6), but for SLD.

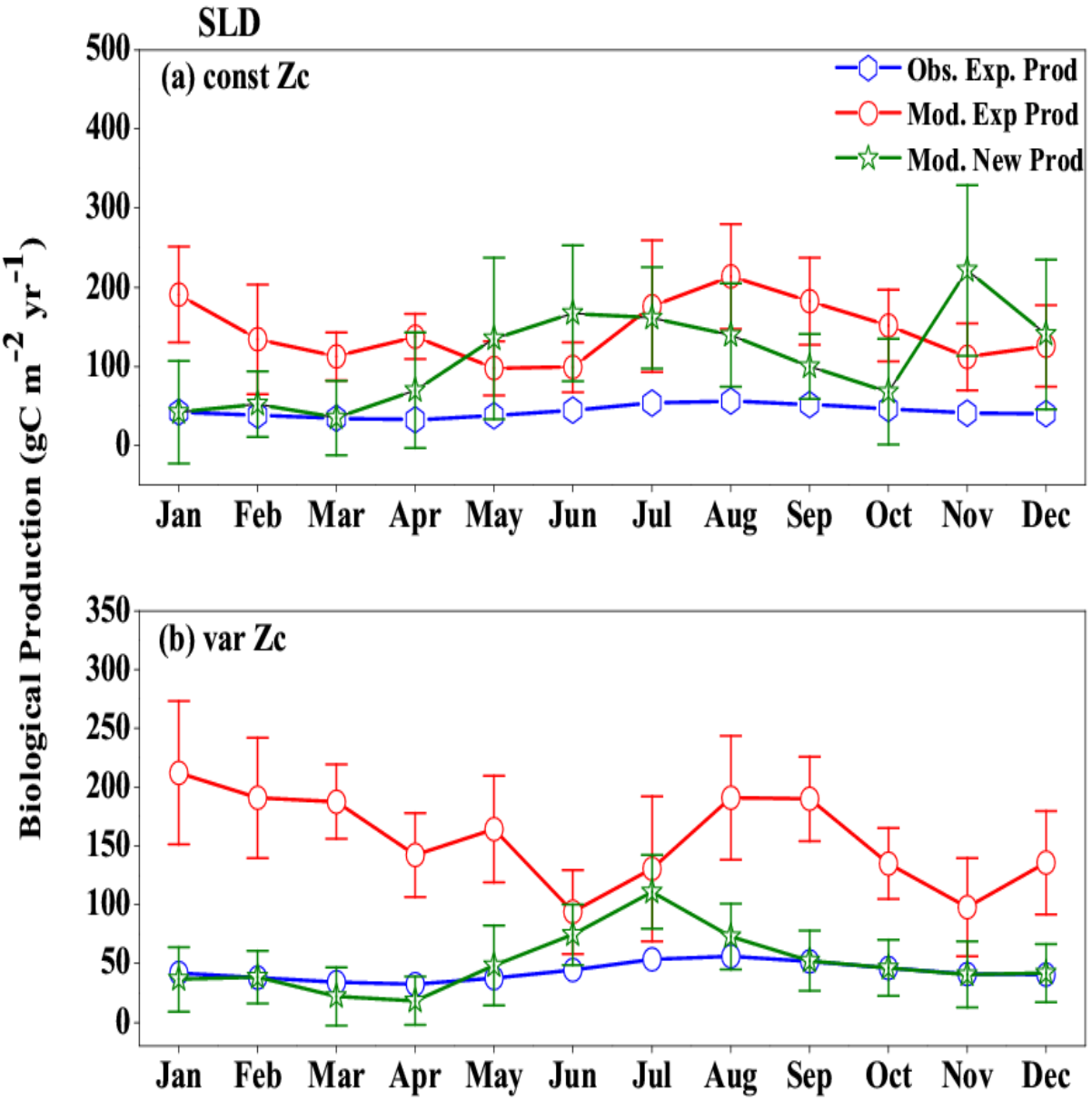

Figure 11: Same as Figure (7), but for SLD.

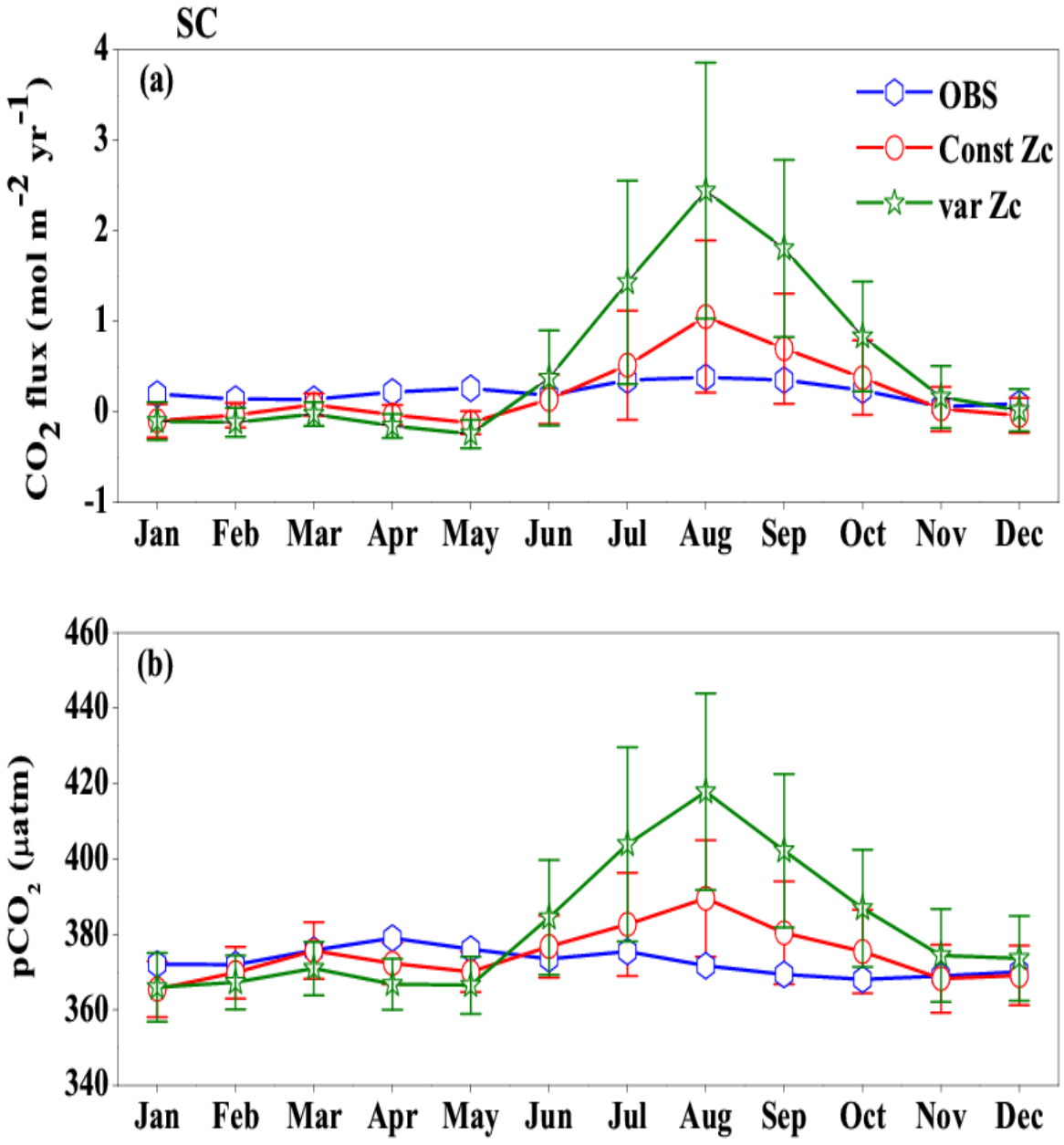

Figure 12: Same as Figure (6), but for SC.

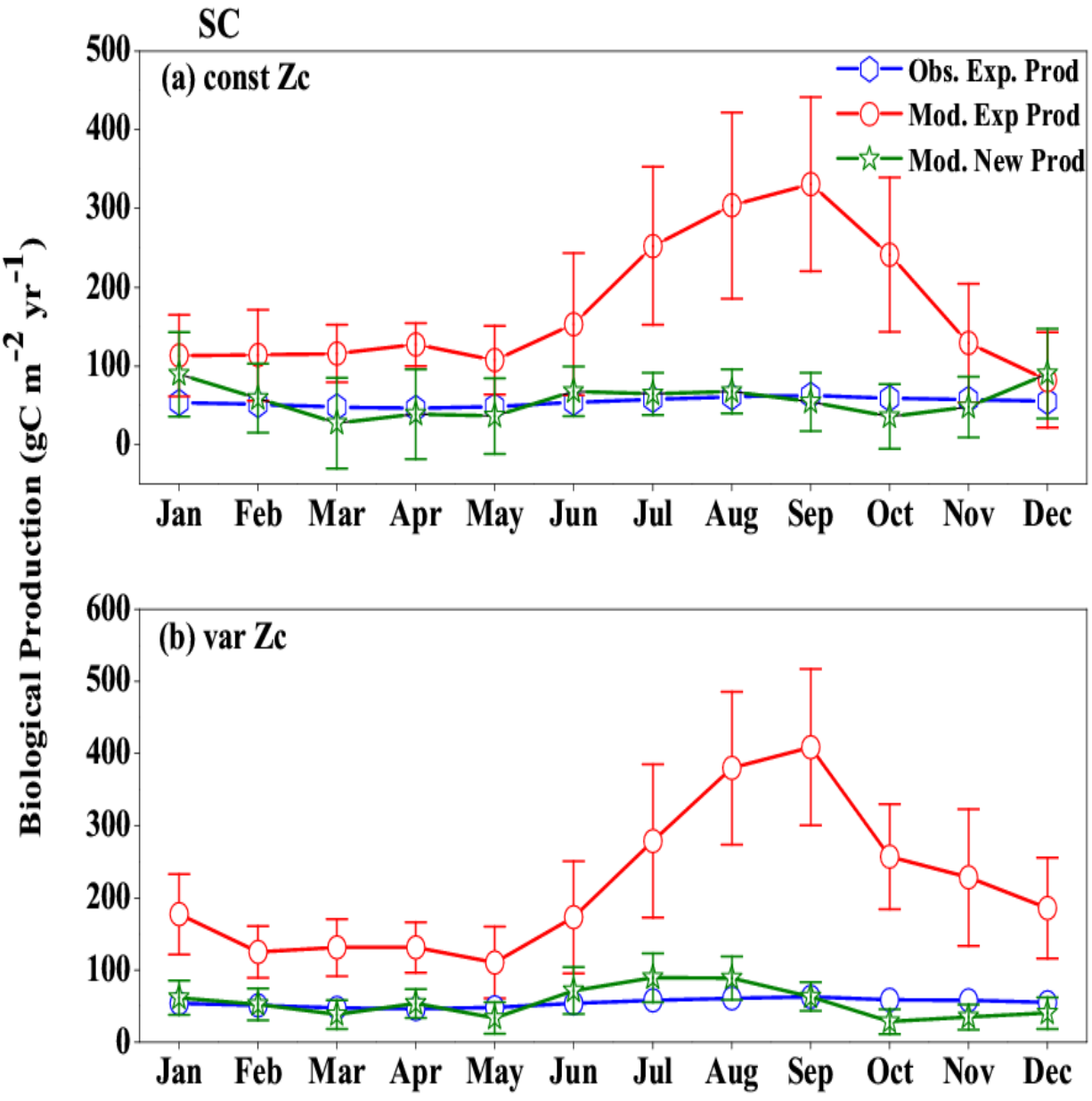

Figure 13: Same as Figure (7), but for SC.

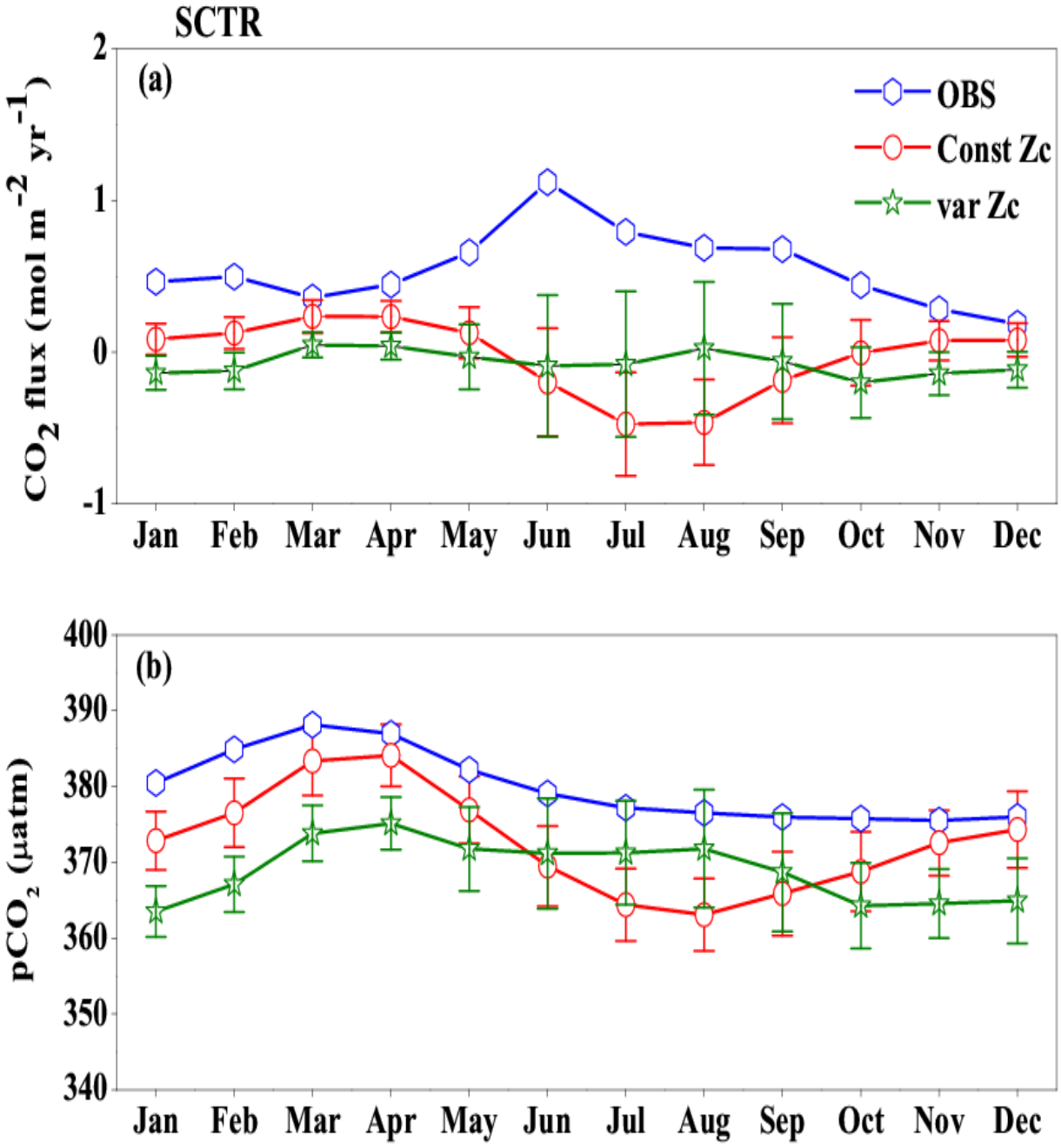

Figure 14: Same as Figure (6), but for SCTR.

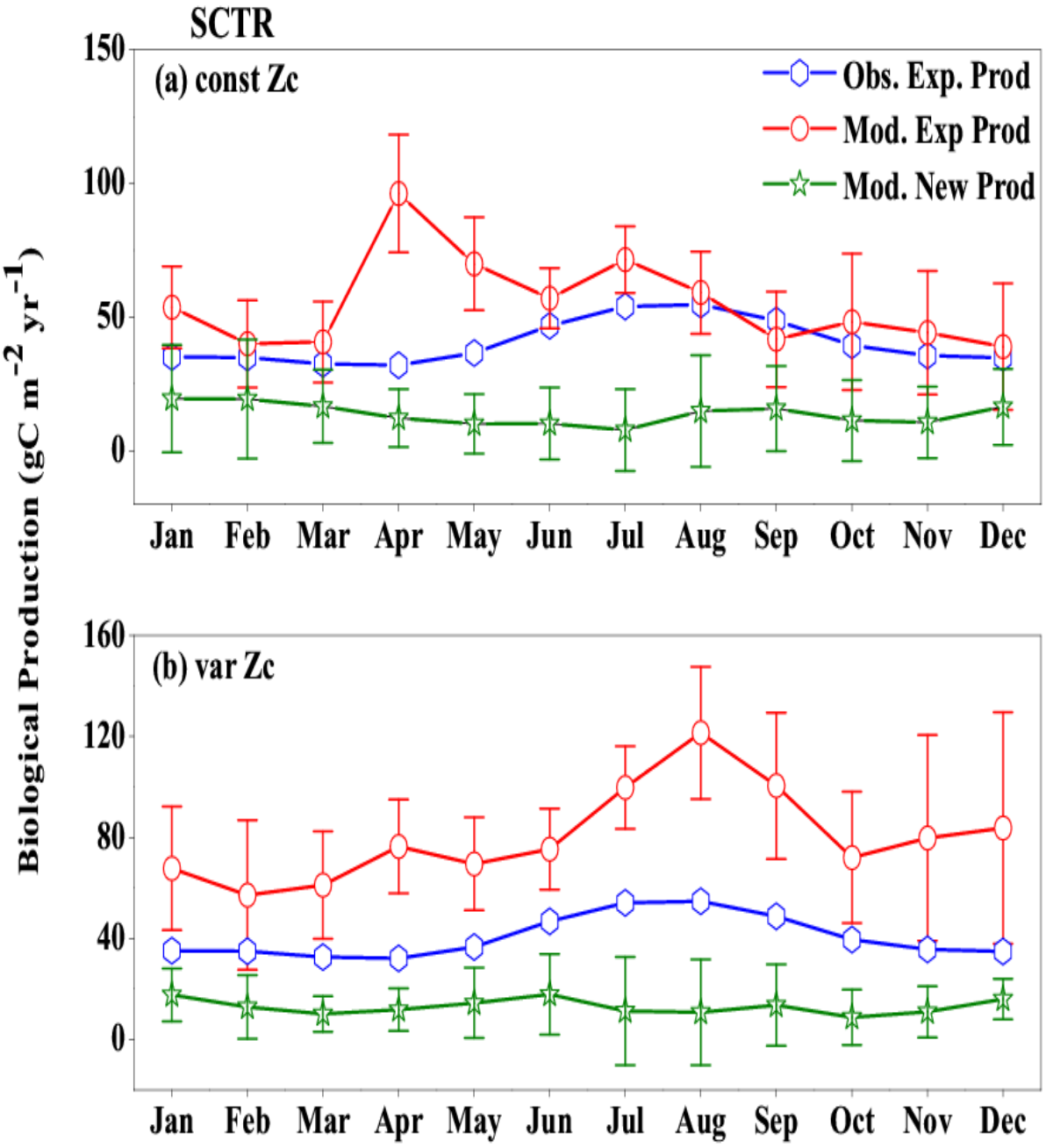

Figure 15: Same as Figure (7), but for SCTR.

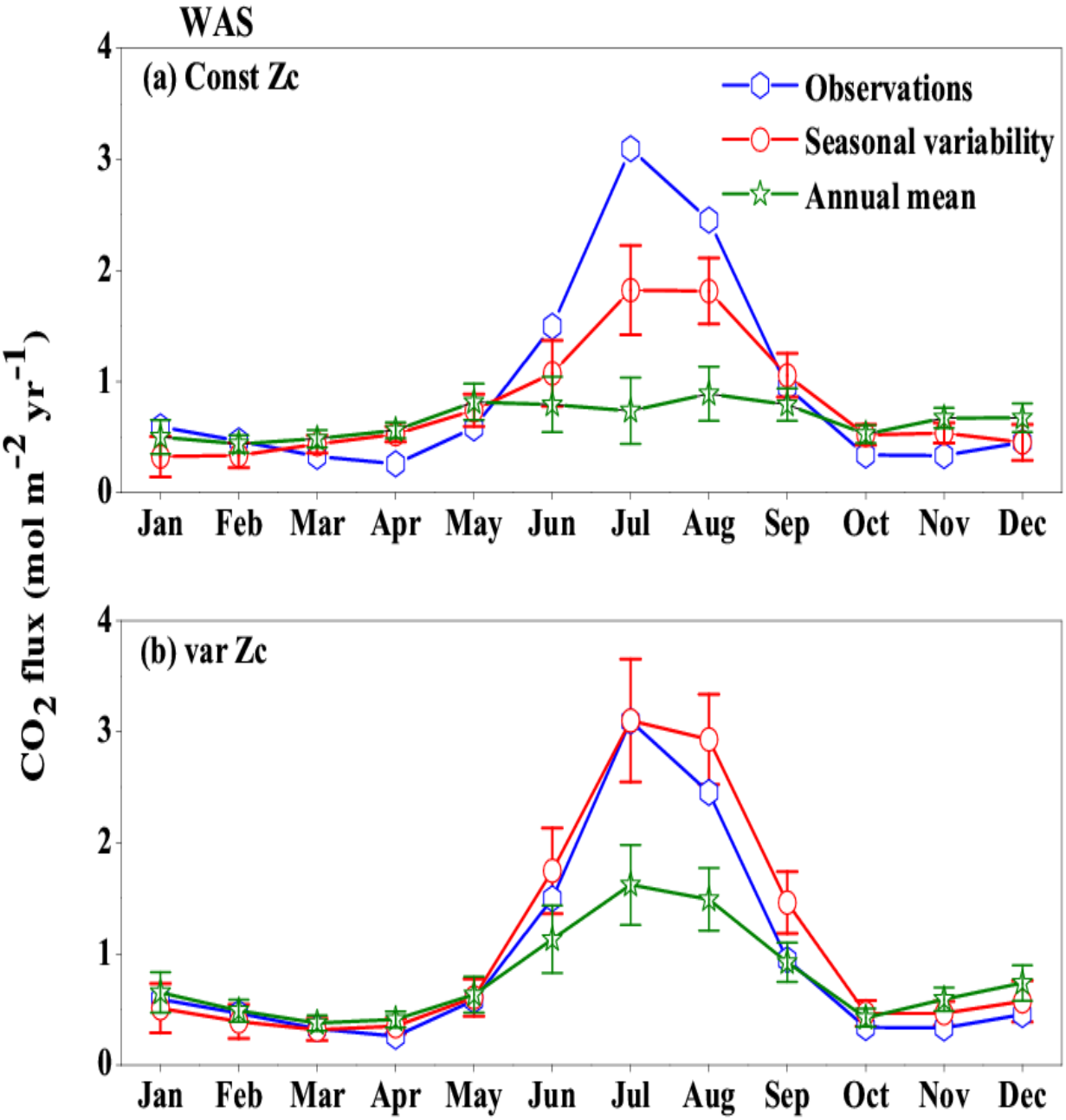

Figure 16: Response of CO_2 flux from the model forced with annual mean currents over the WAS as climatology computed over 1990-2010. Error bar shows standard deviations of individual months over these years. (a) constZc and (b) varZc. Units are mol m^{-2} yr^{-1}. Legends are same for both graphs.

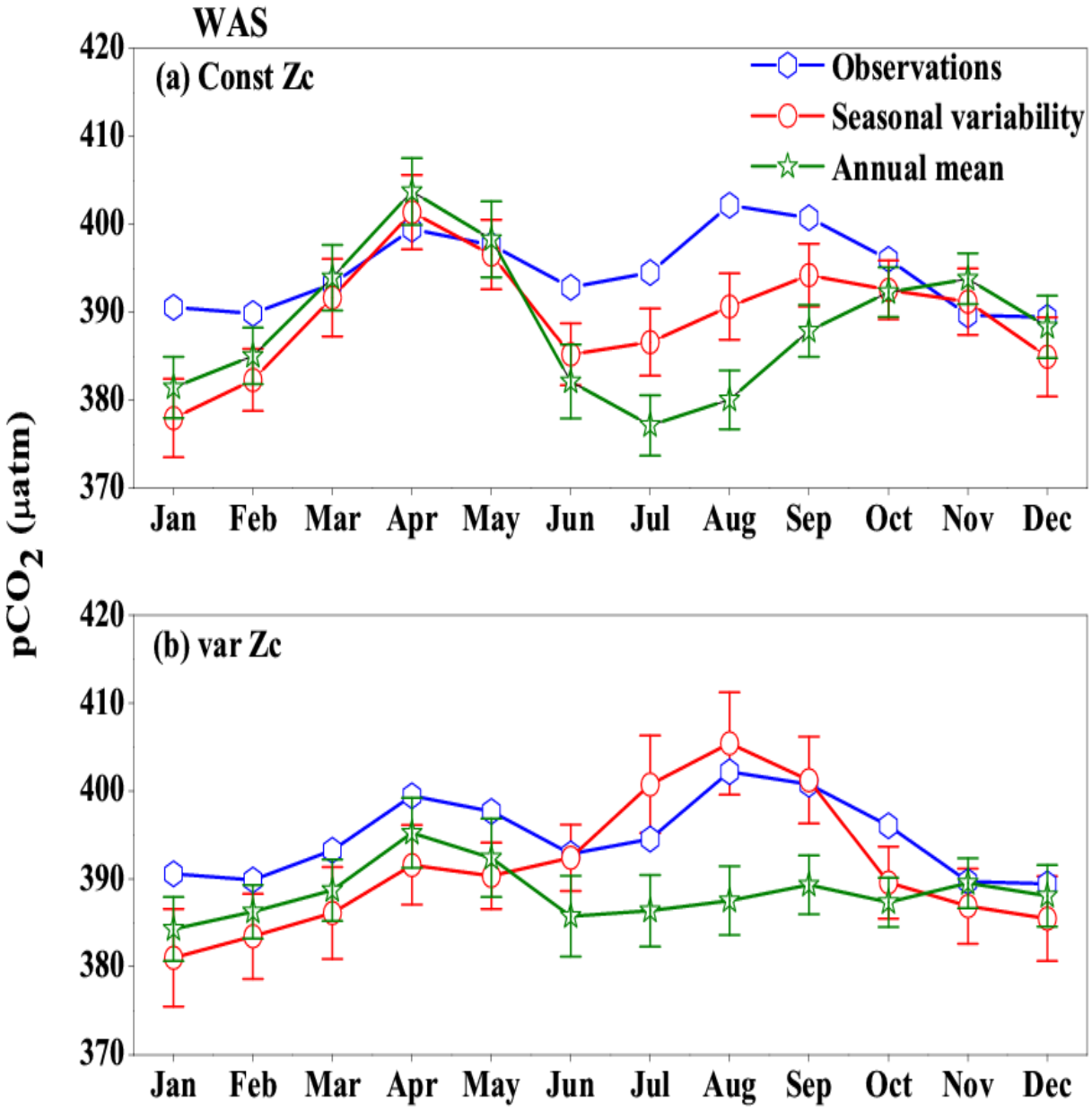

Figure 17: Same as Figure (16), but for pCO_2. Units are µatm.

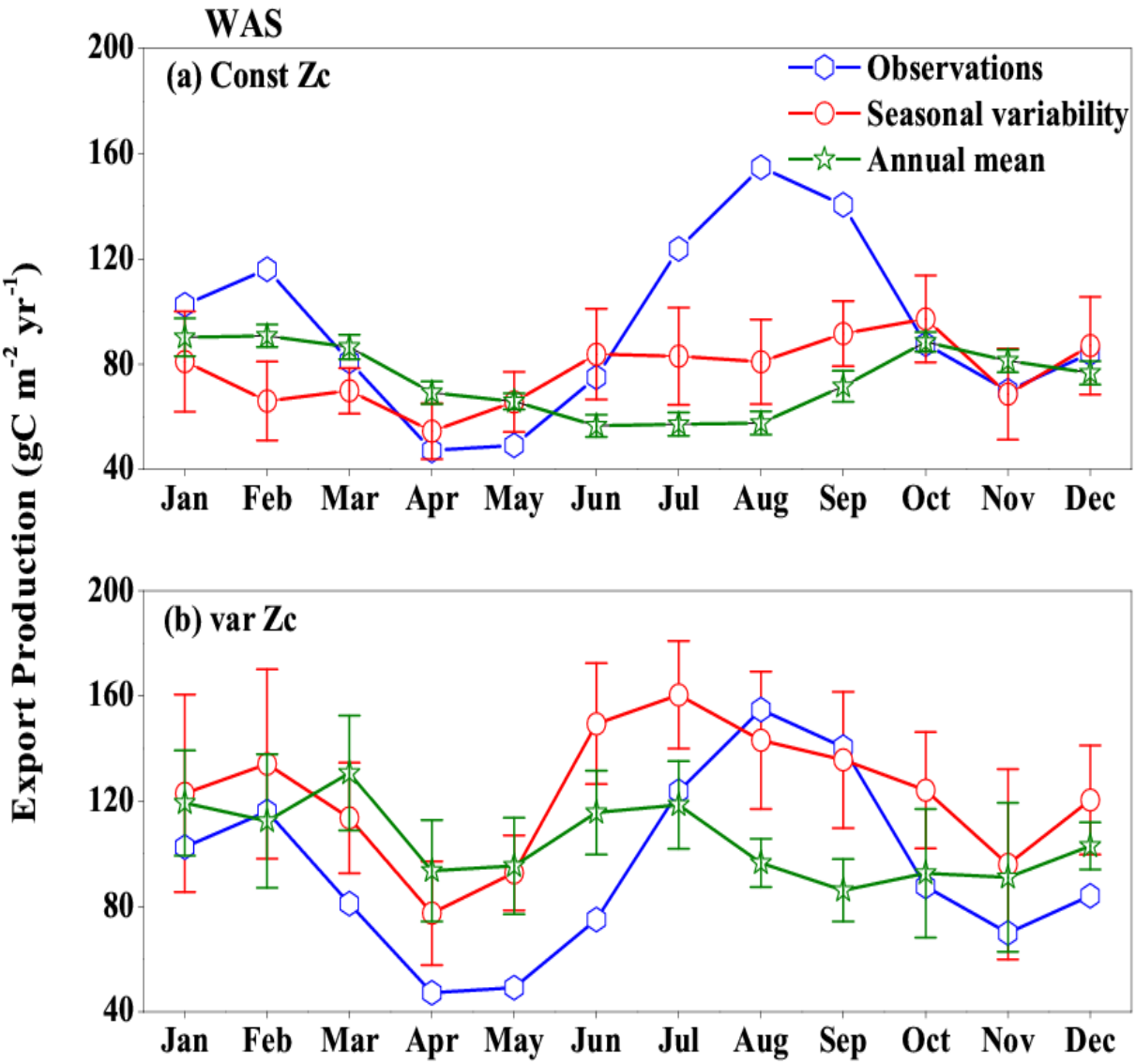

Figure 18: Response in export production of the model forced with annual mean currents in the WAS as climatology computed over 1990-2010. Error bar shows standard deviations of individual months over these years. (a) constZc (b) varZc. Units are g C m^{-2} yr^{-1}. Legends are same for both graphs.

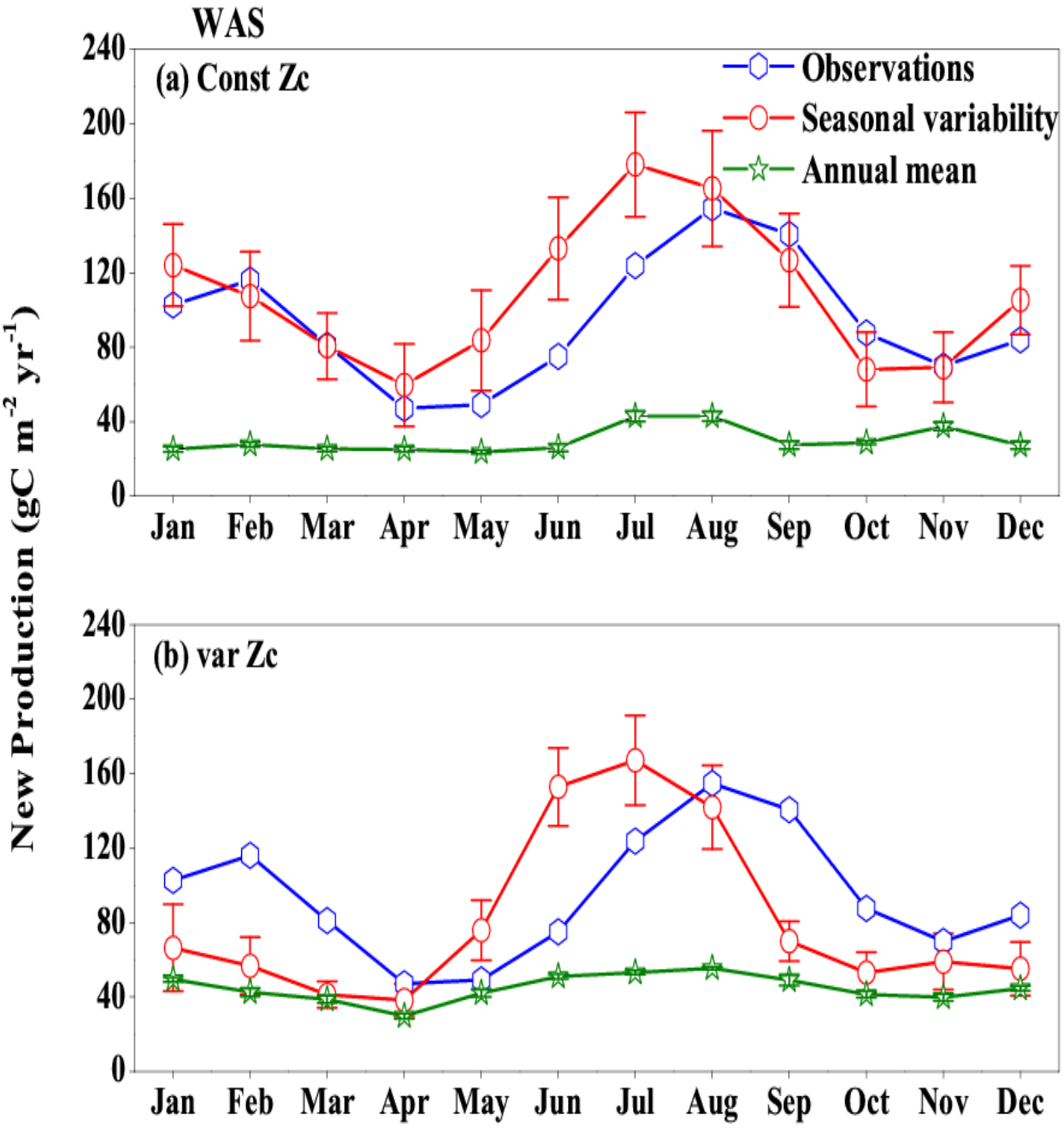

Figure 19: Same as Figure (18), but for New Production. Units are g C m^{-2} yr^{-1}.

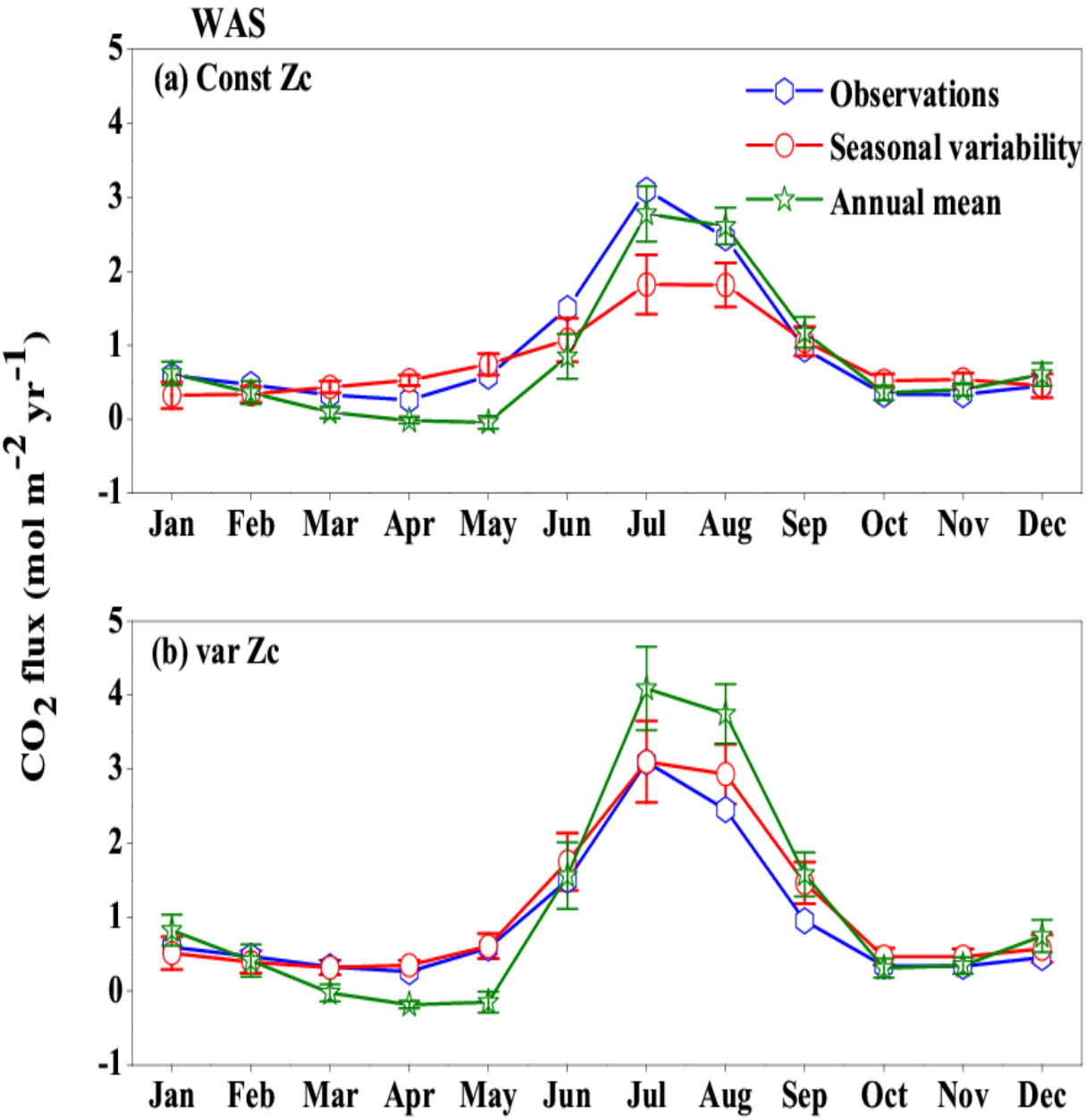

Figure 20: Response of CO_2 flux from the model forced with annual mean SST over the WAS as climatology computed over 1990-2010. Error bar shows standard deviations of individual months over these years. (a) constZc and (b) varZc. Units are mol m^{-2} yr^{-1}. Legends are same for both graphs.

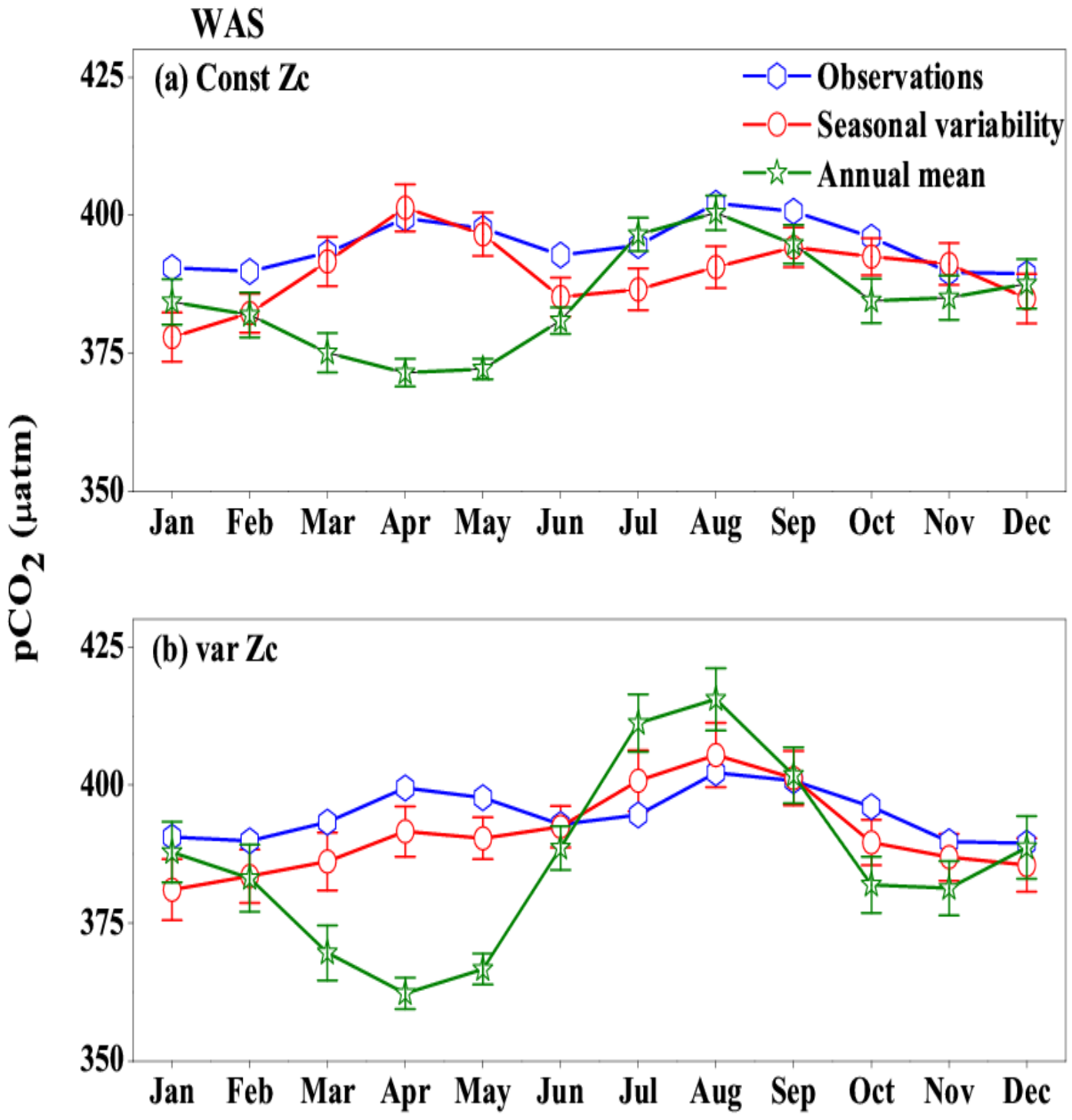

Figure 21: Same as Figure (20), But for pCO_2. Units are µatm.